CANCER

Engineered CD4 TCR T cells with conserved high-affinity TCRs targeting NY-ESO-1 for advanced cellular therapies in cancer

**Margaux Saillard[1,2,3,4,5], Mara Cenerenti[2,3,4,5], Patrick Reichenbach[1,2], Philippe Guillaume[1,2], Ziyang Su[2,3,4,5], Morteza Hafezi[1,2], Julien Schmidt[1,2], Julien Cesbron[1,2], Raphaël Genolet[1,2], Lise Queiroz[1,2], Julien Racle[1,2,6], Jean Villard[7,8], Raffaele Renella[9], Olivier Michielin[10,11], Vincent Zoete[1,2,10], Jean-Paul Rivals[12], Melita Irving[1,2], Daniel E. Speiser[1], Alexandre Harari[1,2], David Gfeller[1,2,6], Olivier Adotevi[13], Francesco Ceppi[9], George Coukos[1,2], Pedro Romero[1,2], Camilla Jandus[1,2,3,4,5]*

While cancer immunotherapy has primarily focused on CD8 T cells, CD4 T cells are increasingly recognized for their role in antitumor immunity. The *HLA-DRB3*02:02* allele is found in 50% of Caucasians. In this study, we screened *HLA-DRB3*02:02* patients with melanoma for tumor-specific CD4 T cells and identified robust New York esophageal squamous cell carcinoma 1 (NY-ESO-1)$_{123–137}$/*HLA-DRB3*02:02* CD4 T cell activity in both peripheral blood and tumor tissue. By analyzing NY-ESO-1$_{123–137}$/*HLA-DRB3*02:02*–restricted CD4 T cell clones, we uncovered an unexpectedly high cytotoxicity, strong T helper 1 polarization, and recurrent αβ T cell receptor (TCRαβ) usage across patients and anatomical sites. These responses were also present in other NY-ESO-1–expressing cancers. TCRs from these clones, when transduced into primary CD4 T cells, showed direct antitumor efficacy both in vitro and in vivo. Our findings suggest that these TCRs are promising for adoptive T cell transfer therapy, enabling broader targeting of NY-ESO-1–expressing adult and pediatric cancers in clinical settings.

INTRODUCTION

Adoptive T cell transfer (ACT) represents a promising, personalized immunotherapy of cancer (*1*). While effector CD8 T lymphocytes are favored for targeting and eliminating malignant cells, emerging evidence suggests that the polyfunctional and cytotoxic subsets of CD4 T cells may be equally crucial in the immune response against cancer (*2*, *3*). In addition, the formation of the cluster of CD8 T cells–CD4 T cells–dendritic cells was shown to be indispensable to overcome CD8 T cell dysfunction upon ACT or immune checkpoint blockade (*4*). Further, case reports have demonstrated that ACT of autologous CD4 T cells enables durable clinical responses in patients with refractory melanoma (*5*) and metastatic epithelial cancer (*6*). Moreover, T cell receptor (TCR)–engineered CD4 T cells targeting tumor antigens, such as MAGE-A3 (melanoma-associated antigen-A3), have shown encouraging tumor regressions following infusion (*7*). The contributions of CD4 in the context of adoptive cell therapy can be multiple, from catalyzing the increased homing of CD8 cytotoxic lymphocytes in tumors to providing critical support to their effector functions. Furthermore, CD4 effector cells may control tumors through stromal targets or direct antitumor cytotoxic function. Nonetheless, several hurdles must be addressed for CD4 T cells to be fully exploited for immunotherapy.

Challenges for CD4 T cell therapies include the high degree of human leukocyte antigen (HLA) polymorphism and diversity of major histocompatibility complex (MHC) class II molecules. This challenge may be limited by focusing on common alleles, such as the *HLA-DRB3*02:02* gene present in half of the Caucasian population (*8*). This would offer a means to identify and target CD4 T cell–defined tumor antigens with a broad coverage of patients with cancer. In addition, the limited cancer specificity of some tumor antigens may result in on-target, off-tumor toxicities [e.g., for TCR T cell targeting of nonmutated antigens such as Melan-A/MART1 (melanoma antigen recognized by T cells), carcinoembryonic antigen, and MAGE-A3] (*9*–*11*). The New York esophageal squamous cell carcinoma 1 (NY-ESO-1) antigen, also known as cancer-testis antigen 1B (*12*), exhibits high mRNA levels in a large number of epithelial cancer types (*13*) but very low levels in normal tissue aside from the testis and ovaries, making it a promising therapeutic target (*12*). Its suitability as a therapeutic target has been confirmed in recent clinical trials, including ACT using NY-ESO-1–specific CD8 T cells and vaccination trials, which have shown promising results, with no observed toxicity (*14*–*17*).

It has further been reported that the NY-ESO-1$_{123–137}$, presented by *HLA-DRB3*02:02*, exhibits high immunogenicity and is immunodominant upon vaccination (*18*). On the basis of these findings, here, we screened *HLA-DRB3*02:02*–positive patients bearing NY-ESO-1–expressing cancers for NY-ESO-1–specific CD4 T cell responses. We observed robust NY-ESO-1$_{123–137}$/*DRB3*02:02* CD4 T cell responses in both peripheral blood and tumor tissue

[1]Department of Oncology UNIL CHUV, University of Lausanne, Lausanne, Switzerland. [2]Ludwig Institute for Cancer Research, Lausanne, Switzerland. [3]Department of Pathology and Immunology, University of Geneva, Geneva, Switzerland. [4]Translational Research Centre in Onco-Hematology (CRTOH), University of Geneva, Geneva, Switzerland. [5]Geneva Centre for Inflammation Research (GCIR), University of Geneva, Geneva, Switzerland. [6]SIB Swiss Institute of Bioinformatics, Lausanne, Switzerland. [7]Division of Nephrology, Geneva University Hospitals, Geneva, Switzerland. [8]Division of Transplantation Immunology, Geneva University Hospitals, Geneva, Switzerland. [9]Pediatric Hematology-Oncology Unit, Division of Pediatrics, Department "Woman-Mother-Child," University Hospital and Lausanne University, Lausanne, Switzerland. [10]Molecular Modeling Group, SIB Swiss Institute of Bioinformatics, Lausanne, Switzerland. [11]Department of Oncology, Geneva University Hospitals, Geneva, Switzerland. [12]Plateforme clinique et translationnelle, Centre des thérapies expérimentales, University Hospital and Lausanne University, Lausanne, Switzerland. [13]Université Bourgogne Franche-Comté, INSERM, EFS BFC, UMR1098, Interactions Hôte-Greffon-Tumeur/Ingénierie Cellulaire et Génique, Besançon, France.
*Corresponding author. Email: camilla.jandus@unige.ch

as compared to other *HLA-DRB3*02:02*–restricted responses including hTERT$_{916–930}$ (human telomerase reverse transcriptase) and Melan-A$_{94–108}$. These naturally occurring NY-ESO-1$_{123–137}$/*DRB3*02:02* CD4 T cells display phenotypic characteristics and functional features within the tumor microenvironment of potent cytotoxic cells that also maintain type 1 cytokine secretion. In addition, the TCR variable chain usage across NY-ESO-1–positive tumor types was highly conserved. On the basis of these intriguing findings, we engineered CD4 T cells with these conserved TCR chain pairs for adoptive therapy. We confirm their antigen specificity and show their strong tumor reactivity, direct cytotoxicity, and ability to control in vivo xenograft tumors upon ACT. Overall, this unique TCR offers promise as a "quasi-universal" TCR and encourages prospects for the treatment of *HLA-DRB3*02:02*–positive adult and pediatric patients with cancer expressing NY-ESO-1.

RESULTS

Several TAA-derived epitopes are immunogenic in an *HLA-DRB3*02:02*–restricted manner

Targeting CD4 T cell–defined antigens presented by *HLA-DRB3*02:02* could address 40% of the population of patients with cancer, a considerable advantage in the face of the extreme polymorphism of HLA-II in humans. To identify novel epitopes restricted by the *HLA-DRB3*02:02* allele, we used the MixMHC2pred algorithm (*19*). Briefly, we searched a panel of clinically relevant tumor associated antigens (TAAs), including MAGE-A1, MAGE-A3, MAGE-A12, hTERT, Melan-A, and mesothelin. Following the initial selection, 15-nucleotide oligomer peptides were scored by MixMHC2pred, generating percent rank scores between 0 and 100, where the lowest values indicated the highest predicted binding to *HLA-DRB3*02:02*. Following initial selection, peptides with a binding score below 3.5 were synthesized alongside NY-ESO-1$_{123–137}$ (*18*) (as detailed in table S1) and tested in vitro to evaluate their immunogenic potential using peripheral blood mononuclear cells (PBMCs) and tumor-infiltrating lymphocytes (TILs)/tumor-infiltrating lymph nodes (TILNs) from multiple *HLA-DRB3*02:02*–positive patients with melanoma and PBMCs from healthy donors (HDs; refer to table S2 for patients' characteristics). The expansion of tumor-specific CD4 T cells was assessed using fluorescent peptide MHCII (pMHCII) multimers (Fig. 1A). As expected, no multimer staining was detected on CD4 T cells derived from *HLA-DRB3*02:02*–negative individuals (Fig. 1B). In contrast, NY-ESO-1$_{123–137}$, Melan-A$_{94–108}$, and hTERT$_{916–930}$/*DRB3*02:02* multimer-positive T cells were readily detected in both PBMCs and TILs/TILNs from *HLA-DRB3*02:02*–positive patients with melanoma, with a trend for higher percentages in TILs/TILNs, albeit at varying frequency depending on the patient (Fig. 1C). Together, these results suggest that the frequently present *HLA-DRB3*02:02* allele efficiently presents immunogenic tumor–derived peptides in both patients with cancer and HDs. In addition, we found two previously unidentified epitopes restricted to the *HLA-DRB3*02:02*, inducing CD4 T cell responses in patients with melanoma.

High cytotoxicity of *HLA-DRB3*02:02*–restricted NY-ESO-1–specific CD4 T cells

To determine the phenotypic and functional attributes of CD4 T cells specific for these epitopes, clones were generated by limiting dilution of sorted pMHCII multimer–positive cells (Fig. 2A). Their cytotoxicity

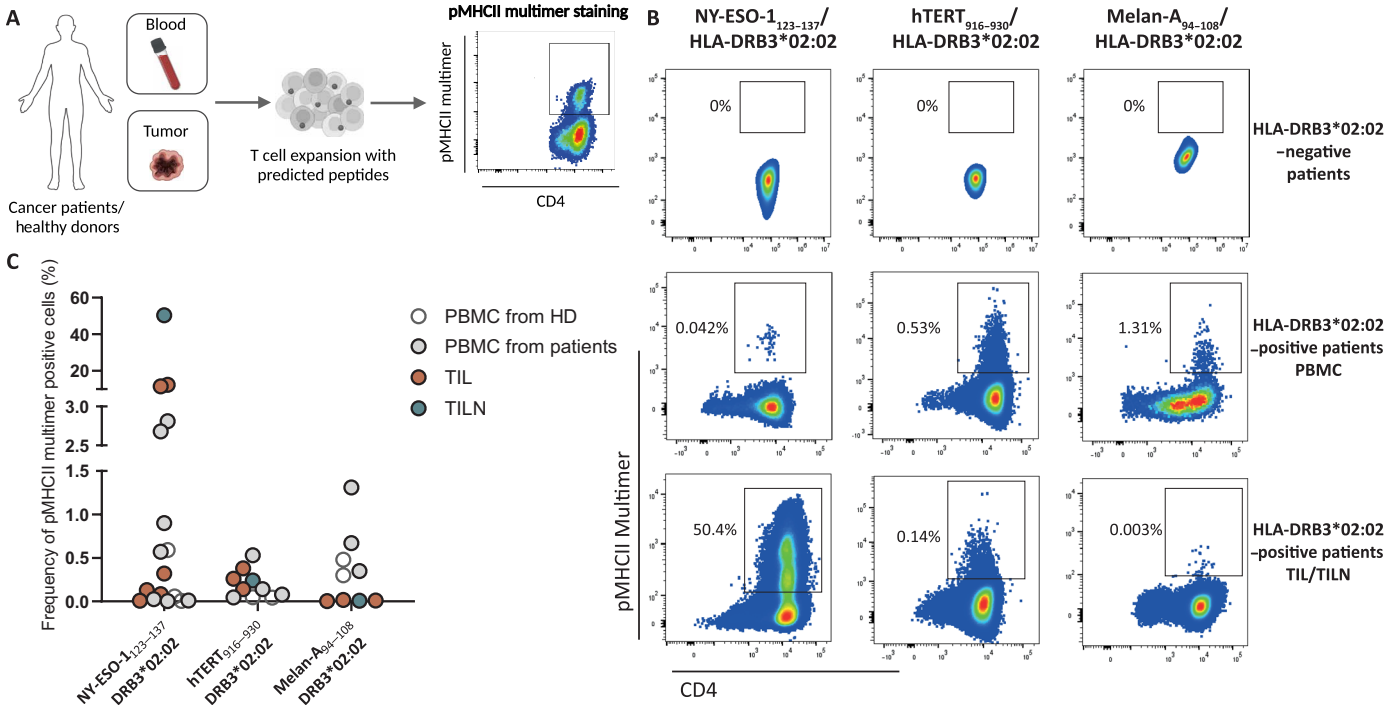

Fig. 1. Detection of antigen-specific CD4 T cells using the pMHCII multimer technology. (**A**) Schematic of the experimental strategy to detect antigen-specific CD4 T cells by pMHCII multimer staining. (**B**) Representative dot plots of pMHCII multimer staining of CD4 T cells specific for NY-ESO-1$_{123–137}$, hTERT$_{916–930}$, and Melan-A$_{94–108}$ in PBMCs and TILs/TILNs of *HLA-DRB3*02:02*$^{+/-}$ patients' and HDs' samples. (**C**) Summarizing graph of antigen-specific CD4 T cell frequencies in PBMCs and TILs/TILNs from patients with melanoma ($n = 8$) and HDs ($n = 3$).

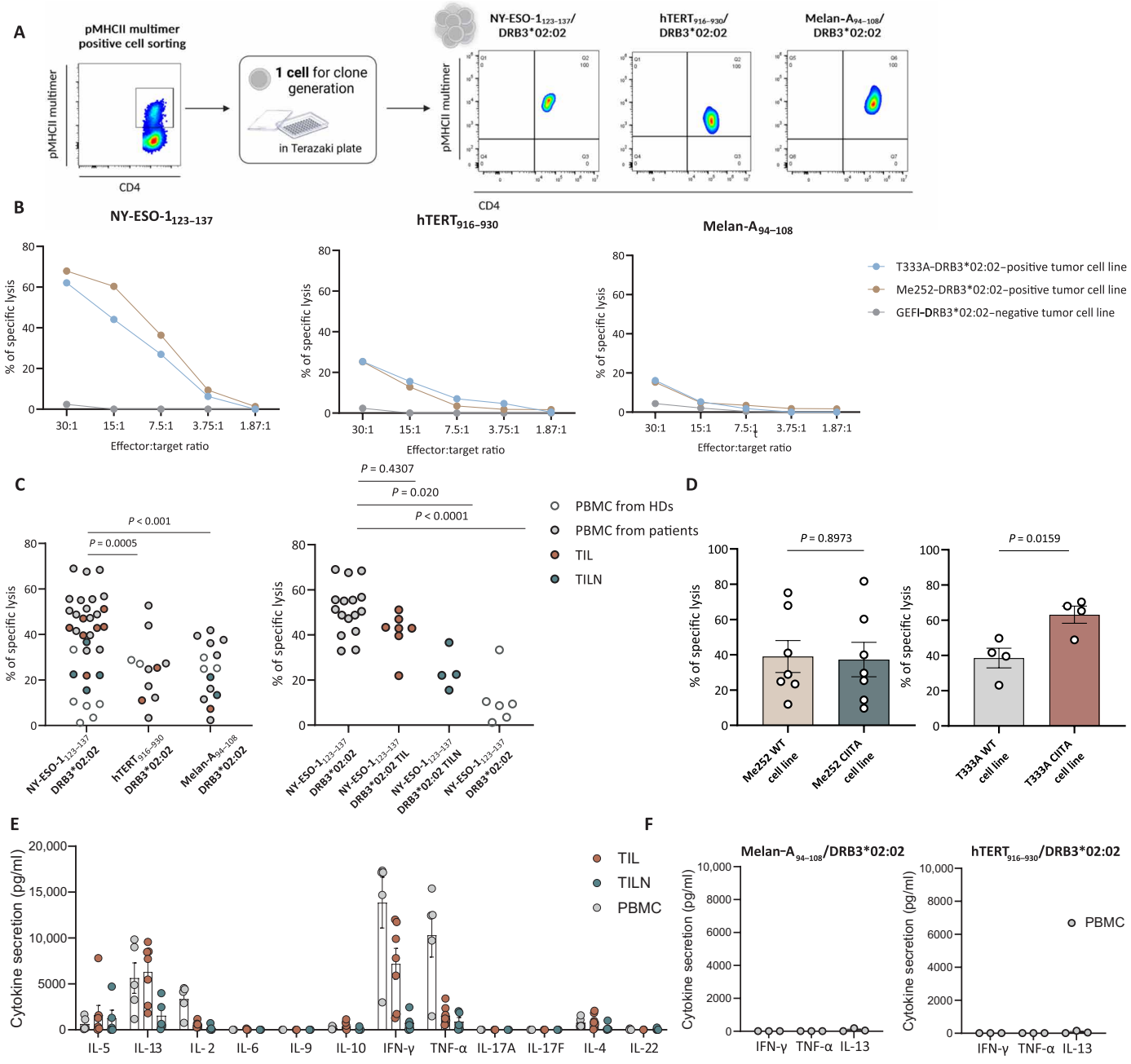

Fig. 2. Cytotoxic potency of diverse tumor antigen–specific CD4 T cells. (**A**) Schematic of the experimental strategy to generate tumor antigen–specific CD4 T cell clones and representative dot plots of NY-ESO-$1_{123–137}$–, hTERT$_{916–930}$–, and Melan-$A_{94–108}$–specific CD4 T cell clones using the pMHCII multimer technology. (**B**) Representative example of the specific lysis using lactate dehydrogenase (LDH) cytotoxic assay conducted with the CIITA-transduced *HLA-DRB3*02:02*$^+$ T333A tumor cell line (in blue), *HLA-DRB3*02:02*$^+$ Me252 tumor cell line (in brown), or *HLA-DRB3*02:02*$^-$ GEFI tumor cell line (in gray) and NY-ESO-$1_{123–137}$–, hTERT$_{916–930}$–, and Melan-$A_{94–108}$–specific CD4 T cell clones. (**C**) Left: Cumulative analysis of LDH cytotoxic assays conducted with tumor cell lines transduced with CIITA and cocultured with NY-ESO-$1_{123–137}$–specific ($n = 33$), hTERT$_{916–930}$–specific ($n = 11$), and Melan-$A_{94–108}$–specific ($n = 14$) CD4 T cell clones (E:T ratio, 30:1). Right: Cumulative analysis of LDH cytotoxic assays conducted with tumor cell lines transduced with CIITA and cocultured with NY-ESO-$1_{123–137}$–specific CD4 T cell clones from PBMCs ($n = 22$), TILs ($n = 7$), and TILNs ($n = 4$) (E:T ratio, 30:1). Statistical power was assessed using one-way analysis of variance (ANOVA). (**D**) Cumulative analysis of LDH cytotoxic assays conducted with tumor cell lines, transduced or not with CIITA, and cocultured with NY-ESO-$1_{123–137}$–specific CD4 T cell clones ($n = 16$) (E:T ratio, 30:1). Statistical power was assessed using *t* test. (**E**) Cumulative data of the maximum values of IFN-γ, TNF-α, IL-4, IL-5, IL-6, IL-9, IL-17A, IL-17F, IL-10, IL-22, and IL-13 secretion obtained in peptide titration experiments using NY-ESO-$1_{123–137}$/*DRB3*02:02* CD4 T cell clones isolated from PBMCs/TILs/TILNs and analyzed by LEGENDplex. (**F**) Cumulative data of the maximum values of IFN-γ, TNF-α, and IL-13 secretion obtained in peptide titration experiment using Melan-$A_{94–108}$–specific CD4 T cell clones ($n = 3$) and hTERT$_{916–930}$-specific CD4 T cell clones ($n = 3$) (right) isolated from PBMCs and analyzed by LEGENDplex.

was assessed against HLA-matched and HLA-mismatched tumor cell lines. To achieve robust and stable MHCII expression on tumor cells, two different *HLA-DRB3*02:02*–positive (T333A and Me252) and one *HLA-DRB3*02:02*–negative (GEFI) melanoma cell line were transduced with the human CIITA (Class II Major Histocompatibility Complex Transactivator) isoform 3 gene (*20*). While the Me252 tumor cell line already constitutively expressed MHCII, the T333A and GEFI tumor cell lines displayed very low basal MHCII expression, which was substantially increased by CIITA transduction (fig. S1). As expected, no specific lysis occurred against *HLA-DRB3*02:02*–negative target cells (Fig. 2B). Unexpectedly, NY-ESO-$1_{123–137}$–specific CD4 T cell clones were highly lytic, achieving up to 72% tumor cell lysis at an effector:target (E:T) ratio of 30:1, whereas Melan-A–specific and hTERT-specific CD4 T cells exhibited low cytotoxic activity. Clones derived from PBMCs of patients demonstrated the highest killing capacity, as compared to clones from tumor-infiltrated tissues. PBMCs of HDs displayed the lowest activity (Fig. 2C). The endogenous expression of MHCII, as in the case of the Me252 cell line, was sufficient to mediate high target cell lysis, while the T333A cell line transduced with CIITA was significantly better killed than the T333A wild-type (WT) cell line, confirming that killing was MHCII dependent (Fig. 2D). Last, we profiled the capacity of the clones to secrete type 1 [interferon-γ (IFN-γ) and tumor necrosis factor–α (TNF-α)], type 2 [interleukin-4 (IL-4), IL-5, and IL-13], type 9 (IL-9), type 17 (IL-17A and IL-17F), and type 22 (IL-6 and IL-22) cytokines and cytotoxic molecules. The maximum effective concentration was determined for each clone (Fig. 2E). NY-ESO-$1_{123–137}$/*DRB3*02:02* CD4 T cell clones secreted high levels of IFN-γ and TNF-α and intermediate levels of IL-13, while prototypic type 9 and type 17/22 cytokines were not significantly produced (Fig. 2E). In addition, TNF-α and IFN-γ secretion was significantly higher in NY-ESO-$1_{123–137}$/*DRB3*02:02* CD4 T cell clones from the PBMCs of patients compared to tumor compartment, arguing for a heightened type 1 polarization of the clones from blood. In contrast, $hTERT_{916–930}$ and Melan-$A_{94–108}$/*DRB3*02:02* CD4 T cell clones did not secrete high levels of IFN-γ, TNF-α, or IL-13, confirming the poor polyfunctional potency of these clones in comparison to the NY-ESO-$1_{123–137}$/*DRB3*02:02* CD4 T cell clones (Fig. 2F). These findings suggest a distinct differentiation path for NY-ESO-$1_{123–137}$–specific clones compared to the other TAA. Melan-A and hTERT/*DRB3*02:02* CD4 T cell clones might be altered in the tumor bed toward a less polyfunctional/effector profile.

To gain insight into the distinctive characteristics of polyfunctional, highly cytotoxic NY-ESO-$1_{123–137}$–specific CD4 T cell clones, we analyzed phenotypic markers and cytotoxic-related molecules released or expressed by NY-ESO-$1_{123–137}$, $hTERT_{916–930}$, and Melan-$A_{94–108}$/*DRB3*02:02* CD4 T cell clones isolated from blood (PBMCs) and tumor (TILs/TILNs) by flow cytometry. Compared to Melan-A–specific and hTERT-specific CD4 T cell clones, patients' clone specific for NY-ESO-$1_{123–137}$ stood out, being 100% positive for PD-1, VISTA, and TIGIT while exhibiting low CD57 expression, regardless of whether they were isolated from blood or tumor tissues (Fig. 3A). In the context of cancer, a higher expression of PD-1, TIGIT, and VISTA in T cells, coupled with low expression of CD57, may suggest an immunosuppressive or exhausted T cell phenotype from chronic antigen exposure. Further, when comparing clones from blood and tumor, we observed a reduction in granzyme B and SLAMF7 expression concomitant to an increase in CTLA-4, OX40, and 41BB expression in TILN/TIL-derived versus PBMC-derived clones, indicating functional exhaustion (Fig. 3B), while the expression of other markers was comparable in both compartments (fig. S2). The increased expression of the last three markers was inversely correlated with the effector capacity of the clones to lyse targets in vitro (Fig. 3C). A similar phenotype was observed on ex vivo multimer-positive CD4 T cells (data not shown).

Strong TCRαβ bias of *HLA-DRB3*02:02*–restricted NY-ESO-1–specific CD4 T cells

To determine whether the TCR repertoire in NY-ESO-$1_{123–137}$–specific cells is oligo/polyclonal and whether it is shared across different compartments (i.e., indicating potential cell migration from the circulation to the tumor bed), we performed TCR sequencing of sorted NY-ESO-$1_{123–137}$–, Melan-$A_{94–108}$–, and $hTERT_{916–930}$–specific CD4 T cell clones. Notably, NY-ESO-$1_{123–137}$–specific CD4 T cell clones derived from three patients' PBMCs ($n = 20$ clones), TILs/TILNs ($n = 19$ clones), or HD PBMCs ($n = 7$ clones) shared a recurrent TCR α variable chain (TRAV), *TRAV8-4* (Fig. 4A). In addition, a TCR β variable chain (TRBV), *TRBV20-1*, was preferentially associated with this TCRα chain across patients. A more diverse set of TCRs was apparent in antigen-specific CD4 T cells from HD, although *TRAV8-4* and *TRBV20-1* were also observed in two of seven HD clones (Fig. 4A). In contrast, Melan-$A_{94–108}$– and $hTERT_{916–930}$–specific CD4 T cell clones restricted by the same *HLA-DRB3*02:02* exhibited diverse TCR usage (Fig. 4A, bottom). In addition, distribution of these recurrent TCR Vα and Vβ chains across individual patients is also highly conserved (fig. S3). Together, these data suggest a potential association between the highly conserved TCR variable chain usage and the observed polyfunctionality traits and high cytotoxicity in *HLA-DRB3*02:02*–restricted NY-ESO-1–specific CD4 T cells. Moreover, Fig. 4A shows that both *TRAV8-4* and *TRBV20-1* are very important for the recognition of the NY-ESO-1 epitope. We determined whether these further preferentially occurred together in the NY-ESO-$1_{123–137}$–specific CD4 T cell clones from patients. For this, we compared the joint probability of these two genes occurring together to the probability in case these were independent {i.e., P(*TRAV8-4* and *TRBV20-1*) ÷ [P(*TRAV8-4*) × P(*TRBV20-1*)] = 1.014}. This value was not significantly higher than when compared to a null model built by randomly pairing the observed *TRAV* and *TRBV* ($P = 0.106$), indicating that, despite the high frequency of both TRAV8-4 and TRBV20-1 in TCRs recognizing NY-ESO-1, these two genes are selected independently of each other and are not jointly needed for the recognition of NY-ESO-1 (as can be seen by the NY-ESO-1–specific TCRs formed by *TRBV8-4/TRBV11-2* or *TRBV19/TRBV20-1*, for example). To assess whether the dominance of these TCRα and TCRβ chains resulted from antigen-independent activation upon in vitro culture, NY-ESO-$1_{123–137}$ multimer-positive and multimer-negative cells were sorted from in vitro–expanded PBMCs and TILs/TILNs from *HLA-DRB3*02:02*–positive patients (Fig. 4B), and TCR usage was analyzed on these bulk cultures. Across nine patients with melanoma, we observed this highly conserved TCR variable chain, *TRAV8-4*, within the multimer-positive T cells, representing more than 50% of all the TCR chains observed but not in the multimer-negative T cells (Fig. 4B). In addition, *TRBV20-1* was only preferentially used in the multimer-positive cells (Fig. 4B). Last, to definitively rule out a preexisting, natural selection–derived bias toward TRAV8-4 and TRBV20-1 in human CD4 T cells in general, we sequenced TCRs from cord blood–derived naïve CD4 T cells and compared them to bulk memory CD4 T cells from adult individuals (Fig. 4C). Neither *TRAV8-4* nor *TRBV20-1* was identified among the most frequently expressed TCRs in CD4 T cell from three cord

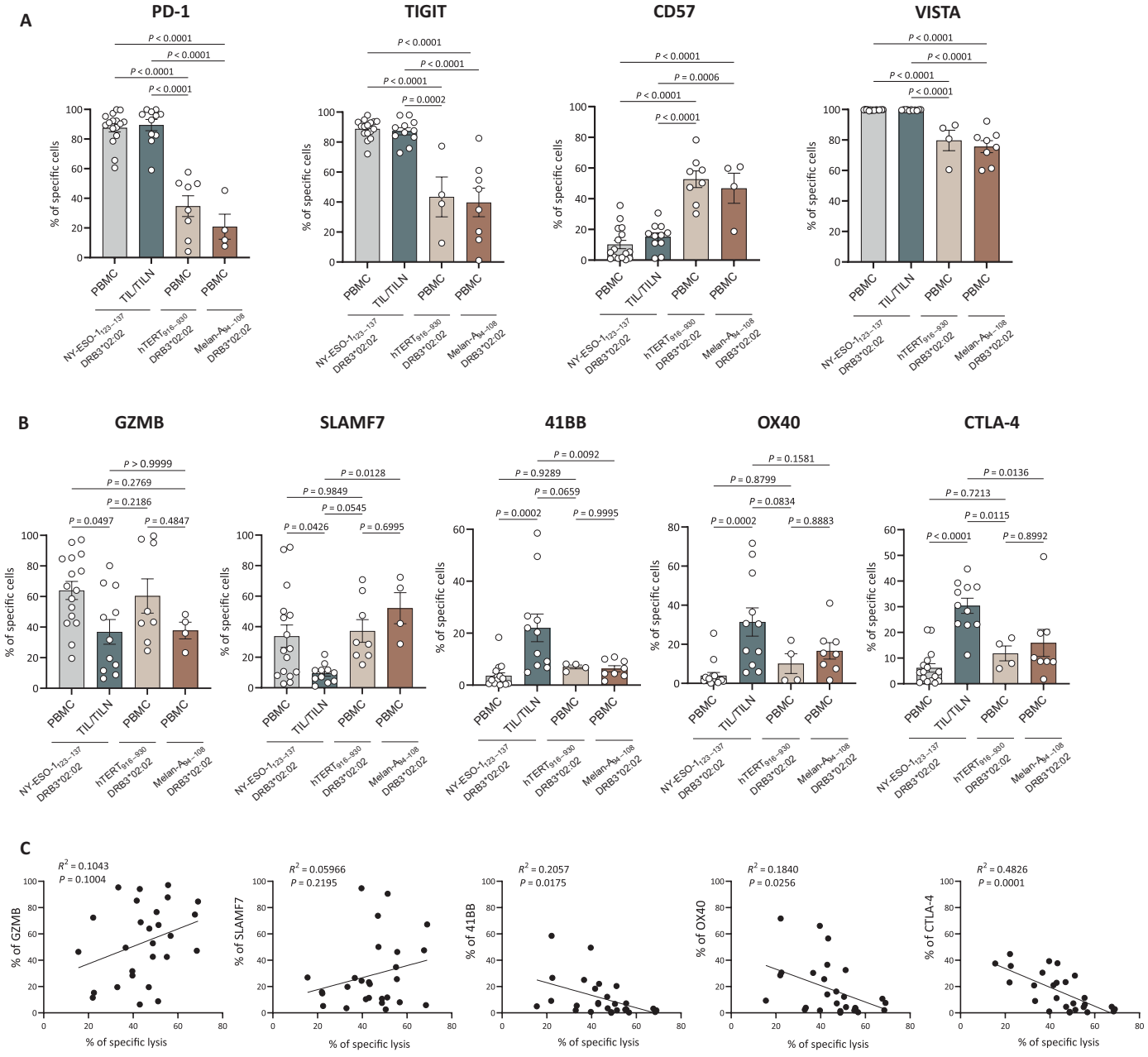

Fig. 3. Phenotypic characterization of diverse tumor antigen–specific CD4 T cells. (**A**) Graphs summarizing PD-1, TIGIT, CD57, and VISTA expression in NY-ESO-$1_{123–137}$ PBMC–specific ($n = 16$), TIL/TILN–specific ($n = 11$), hTERT$_{916–930}$ PBMC–specific ($n = 8$), and Melan-$A_{94–108}$ PBMC–specific ($n = 4$) CD4 T cell clones. Statistical power was assessed using one-way ANOVA. (**B**) Graphs summarizing GZMB, SLAMF7, OX40, 41BB, and CTLA-4 expression in NY-ESO-$1_{123–137}$ PBMC–specific ($n = 16$), TIL/TILN–specific ($n = 11$), hTERT$_{916–930}$ PBMC–specific ($n = 8$), and Melan-$A_{94–108}$ PBMC–specific ($n = 4$) CD4 T cell clones. Statistical power was assessed using one-way ANOVA. (**C**) Graphs summarizing the correlation between the percentage of specific lysis of NY-ESO-$1_{123–137}$–specific CD4 T cell clones and GZMB, SLAMF7, 41BB, OX40, and CTLA-4 ($n = 27$). Statistical power was assessed using simple linear regression.

blood samples and four adult memory cells (Fig. 4D). The overall usage of TRAV8-4 and TRBV20-1 was similar in human multimer–negative CD4 T cells of patients, PBMCs of healthy individuals, and fetal cord blood. These results support a selective usage of TCR variable chains: TRAV8-4/TRBV20-1 in highly cytotoxic *DRB3*02:02*-restricted NY-ESO-1–specific CD4 T cells.

To determine the possible origin of the TCR preference in the NY-ESO-1/*HLA-DRB3*02:02* response, we generated, by homology modeling, three-dimensional (3D) structural models of *HLA-DRA* + *HLA-DRB3*02:02* in complex with the NY-ESO-1, hTERT, or Melan-A peptide of interest, as well as these three pMHCs in complex with three distinct NY-ESO-1–specific CD4 TCRs with a TCR alpha chain bias (i.e., TCR1, TCR2, and TCR3) (table S3). Following a previously described approach using the Modeller and TCRmodel2 programs (*21*, *22*), we identified and enumerated molecular interactions existing in these 3D structural models between

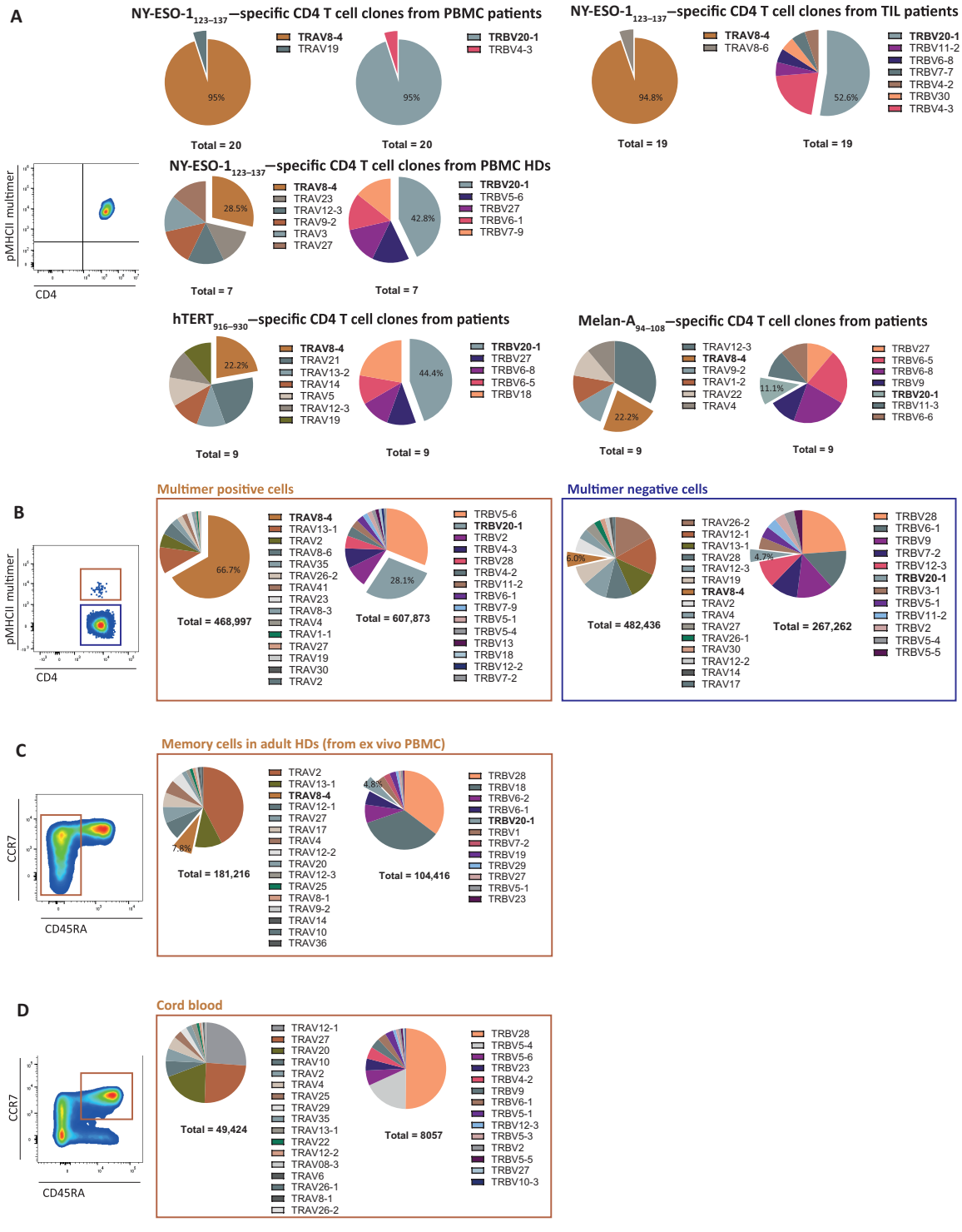

Fig. 4. Highly conserved TCR Vα and TCR Vβ usage in NY-ESO-1$_{123–137}$/*DRB3*02:02*–specific CD4 T cells. (**A**) Pies illustrating the relative abundance of each clonotype among all NY-ESO-1$_{123–137}$/*DRB3*02:02* CD4 T cell clones in the PMBCs ($n = 20$) and TILs/TILNs ($n = 19$) of patients with melanoma and HDs' PBMCs ($n = 7$), Melan-A$_{94–108}$ ($n = 9$), and hTERT$_{916–930}$/*DRB3*02:02* ($n = 9$) CD4 T cell clones. (**B**) Pies summarizing TCR sequencing of the alpha and beta chains of multimer-positive (left pies) or multimer-negative (right pies) CD4 T cells sorted from in vitro–expanded PBMCs and TILs/TILNs from patients ($n = 9$). (**C**) Pies summarizing TCR sequencing of the alpha and beta chains of memory CD4 T cells isolated from adult blood ($n = 4$). (**D**) Pies summarizing TCR sequencing of the alpha and beta chains of naïve CD4 T cells isolated from cord blood ($n = 3$).

each peptide and the MHC and between each NY-ESO-1 TCR and the different pMHCs. Results are summarized in Table 1. The nature of the molecular interactions existing between the peptide, MHC, and TCR residues is listed in tables S4 to S15.

NY-ESO-1 was predicted to make substantially more interactions with *HLA-DRA* and *HLA-DRB3*02:02* (a total of 43) than hTERT (37) or Melan-A (35) and, hence, may have a stronger affinity for this MHC than hTERT and Melan-A. Furthermore, TCR1, TCR2, and TCR3 were predicted to make a similar number of favorable molecular interactions with the NY-ESO-1 peptide, as well as to make more favorable interactions with the NY-ESO-1 than with hTERT or Melan-A. Notably, TCR1 makes a higher number of favorable molecular interactions with *HLA-DRB3*02:02* than TCR2 or TCR3. Overall, the TCR1/NY-ESO-1/*HLA-DRA* + *HLA-DRB3*02:02* complex (Fig. 5) was predicted to exhibit the largest number of favorable molecular interactions between all partners. These findings suggest a potential specificity or affinity difference in the recognition of these pMHC complexes by the analyzed TCRs, which might drive their preferential expansion and effector functions.

Enriched NY-ESO-1–specific TCR-biased CD4 T cells across human tumor types

NY-ESO-1 is a TAA expressed by a broad range of tumor types. Hence, we questioned whether NY-ESO-$1_{123–137}$–specific CD4 T cells with the described TCR bias can also be detected in cancers other than melanoma, such as lung cancer, ovarian cancer, and neuroblastoma. Targeting a broad spectrum of pediatric and adult tumor types by the same strategy would be therapeutically highly relevant. TCR analysis was performed after one round of stimulation with the NY-ESO-1 peptide. As shown in Fig. 6 (A to C), we detected NY-ESO-$1_{123–137}$/*DRB3*02:02* CD4 T cells in samples from patients with lung, ovarian, and neuroblastoma cancer (see table S2 for patients' characteristics). In patients with lung cancer, we also observed highly conserved TRAV8-4 usage. In contrast, in patients with ovarian and neuroblastoma cancer, TRBV20-1 but not TRAV8-1 was highly conserved, suggesting that the usage of this TCR by NY-ESO-$1_{123–137}$/*DRB3*02:02* CD4 T cells is a partially generalized feature, not restricted to patients with melanoma (Fig. 6).

Expression of NY-ESO-1–specific TCRs reprograms antitumor activity in primary human CD4 T cells in vitro and in vivo

Next, to evaluate a possible therapeutic application of this highly conserved TCR variable chain usage, we transduced different TCRs in human primary CD4 T cells using a lentiviral vector in combination with CRISPR-Cas9 genetic deletion of the endogenous TCR (Fig. 7A). Strong transduction efficiency (Fig. 7B) and cell survival (Fig. 7C) were better in primary CD4 T cells. Lower levels of tetramer staining were observed for transduced CD8 T cells, indicating that these TCRs may be CD4 dependent. Transduced CD4 T cells exerted strong *HLA-DRB3*02:02*–positive tumor cell lysis, while, as expected, no cytotoxicity was measured against *HLA-DRB3*02:02*–negative ones (Fig. 7D). NY-ESO-$1_{123–137}$–specific CD4 T cells exhibited a bias toward a T helper type 1 and 2 phenotype, producing IL-2, IFN-γ, TNF-α, IL-5, and IL-13 upon recognition of *HLA-DRB3*02:02*–positive tumors (Fig. 7E). No cytokine secretion was observed when cocultured with *HLA-DRB3*02:02*–negative tumors.

We next sought to evaluate CD4 T cells engineered to express NY-ESO-1/TCRs having the best predictive pMHC/TCR affinity

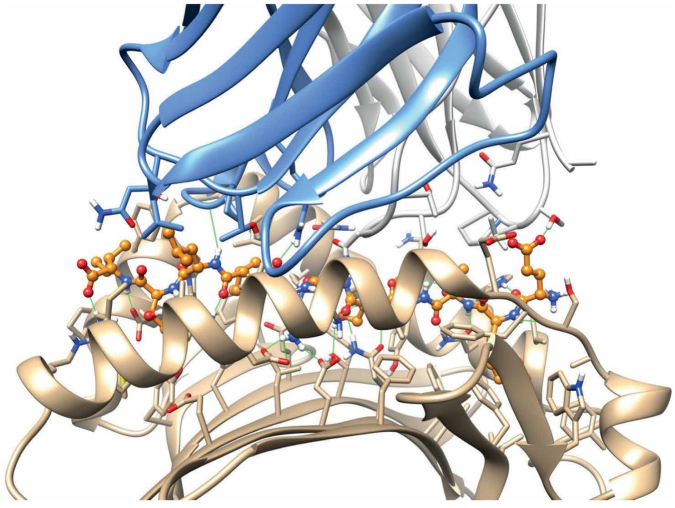

Fig. 5. 3D structural model obtained using TCRmodel2 for the complex TCR1/NY-ESO-1/*HLA-DRA* + *HLA-DRB3*02:02*. TCR1 is colored gray (TCRα) and blue (TCRβ), *HLA-DRA* and *HLA-DRB3*02:02* are colored brown, and NY-ESO-1 is colored orange. Residues of the peptide are displayed in ball-and-stick representation, while those of the MHC and TCR are shown in stick representation. Hydrogen bonds are shown as thin green lines. Nonpolar hydrogens are hidden for clarity.

Table 1. Number of favorable molecular interactions between the peptide and the MHC, as well as between the TCRs and the peptide or the MHC, determined from the nine structural models of the pMHC and TCR-pMHC complexes.

Complex	No. of interactions, Pep/MHC	No. of interactions, TCR/Pep	No. of interactions, TCR/MHC	Total
TCR1-NY-ESO-1-*HLA-DRB3*02:02*	43	10	30	83
TCR2-NY-ESO-1-*HLA-DRB3*02:02*	43	11	26	80
TCR3-NY-ESO-1-*HLA-DRB3*02:02*	43	11	24	78
TCR1-hTERT-*HLA-DRB3*02:02*	37	9	29	75
TCR2-hTERT-*HLA-DRB3*02:02*	37	7	28	72
TCR3-hTERT-*HLA-DRB3*02:02*	37	8	22	67
TCR1-MelanA-*HLA-DRB3*02:02*	35	9	28	72
TCR2-Melan-A–*HLA-DRB3*02:02*	35	8	26	69
TCR3-Melan-A–*HLA-DRB3*02:02*	35	9	25	69

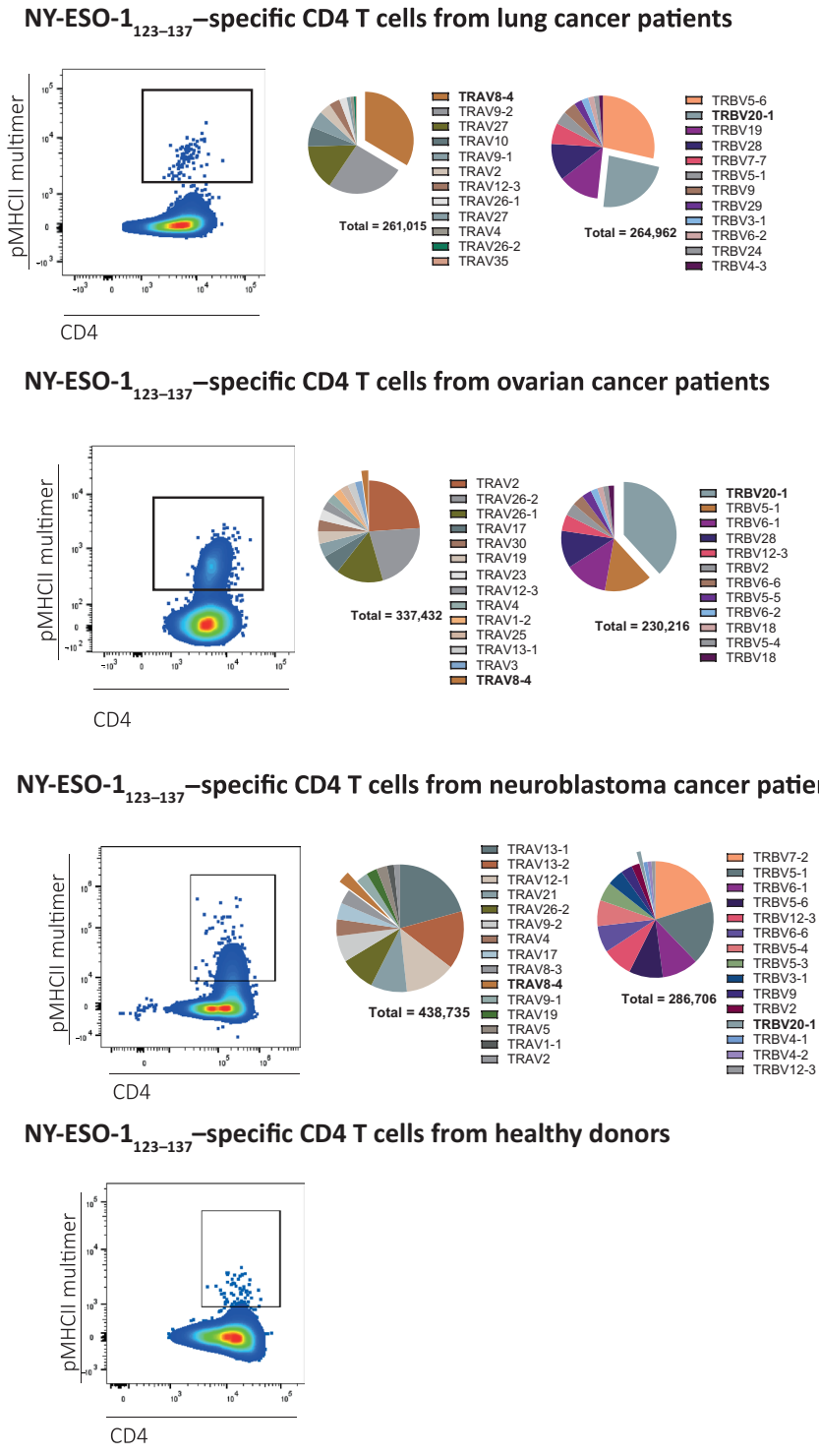

Fig. 6. NY-ESO-1$_{123–137}$–specific CD4 T cells in other tumor types. Representative dot plots and pies summarizing TCR alpha and beta chains of multimer-positive CD4 T cells after in vitro stimulation with the NY-ESO-1$_{123–137}$ peptide in (**A**) samples from patients with lung cancer ($n = 5$), (**B**) samples from patients with ovarian cancer ($n = 3$), (**C**) samples from patients with neuroblastoma pediatric cancer ($n = 3$), and (**D**) healthy donor samples.

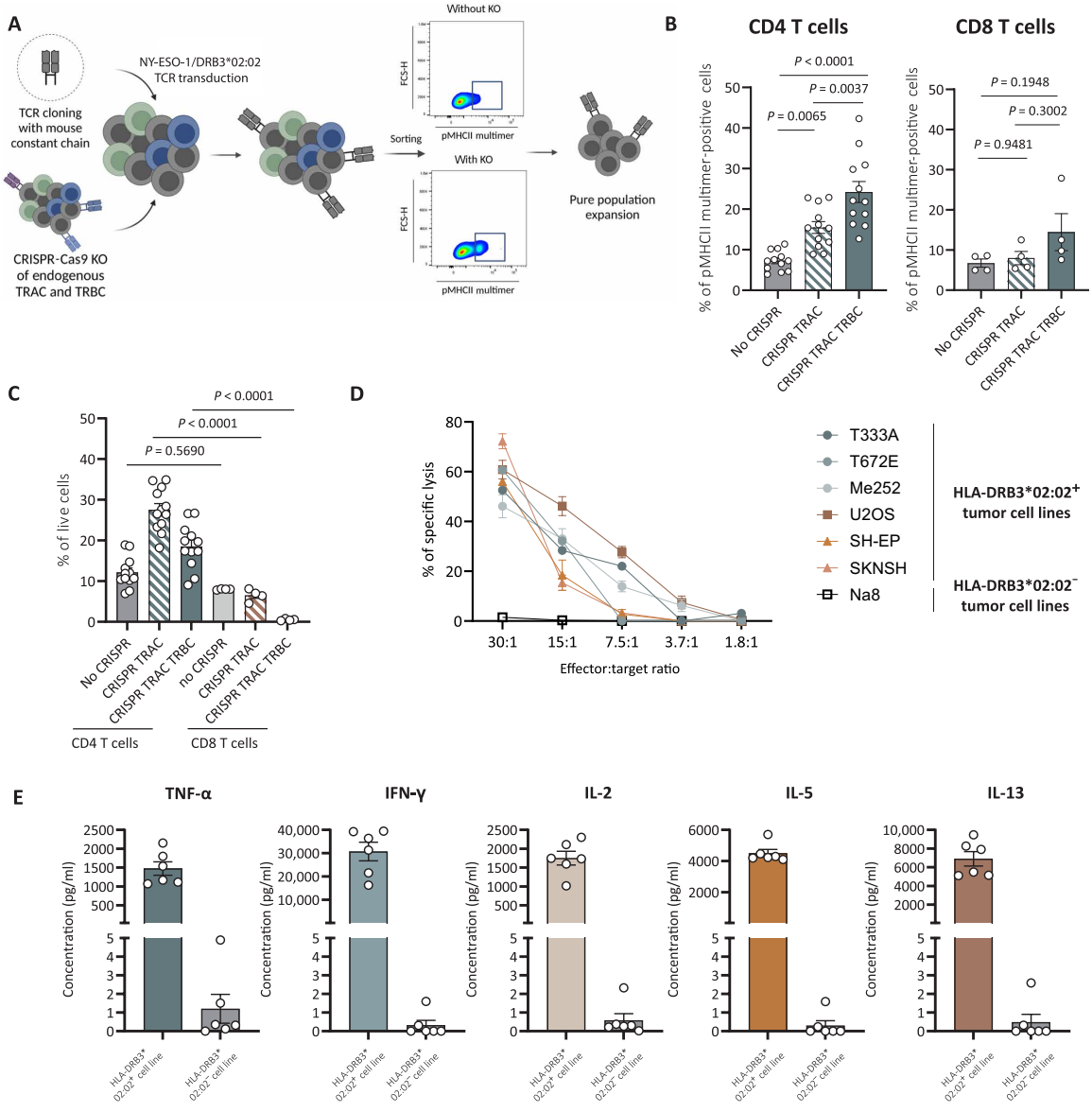

Fig. 7. TCR transduction in human primary CD4 T cells. (**A**) Schematic of experimental strategy to generate NY-ESO-1/TCR–transduced human CD4 T cells. KO, knockout. (**B**) Cumulative analysis of TCR transduction in CD4 ($n = 12$) and CD8 ($n = 4$) T cells, with or without CRISPR editing. Statistical power was assessed using one-way ANOVA. (**C**) Cumulative analysis of percentage of live cells in TCR-transduced CD4 ($n = 12$) or CD8 ($n = 4$) T cells, with or without CRISPR editing. Statistical power was assessed using one-way ANOVA. (**D**) Cytotoxic capacity of TCR-transduced CD4 T cells against different HLA-matched and HLA-mismatched tumor cell lines (E:T ratio, 30:1) ($n = 4$). (**E**) Cytokine secretion analysis (TNF-α, IFN-γ, IL-2, IL-5, and IL-13) by LEGENDplex in supernatants of NY-ESO-$1_{123–137}$/TCR–transduced CD4 T cells for the higher ratio E:T (30:1) ($n = 6$).

(Table 1) in vivo. Briefly, after tumor engraftment in immunodeficient IL-2–NOG (NOD/Shi-scid/IL-2Rγnull) mice (*23*), ACT was performed with TCR-transduced NY-ESO-$1_{123–13}$/*DRB3*02:02*–specific CD4 T cells or with TCR-transduced NY-ESO-$1_{157–165}$/*HLA-A2*02:01*–specific CD8 T cells (Fig. 8A). As shown in Fig. 8B, NY-ESO-$1_{123–137}$/*DRB3*02:02*-TCR–transduced primary CD4 T cells could control tumor growth as efficiently as NY-ESO-$1_{157–165}$/HLA-A*02:01-TCR–transduced CD8 T cells, in comparison to the untreated group where the tumors grew uncontrolled. To assess the persistence of transferred T cells, we monitored the number of circulating human $CD3^+$ T cells by flow cytometry in three different groups (Fig. 8, C and D). As expected, no human CD3 cells were observed in untreated mice. In contrast, we obtained similar $CD3^+$ cell counts for both treated groups, demonstrating the persistence (tested up to 33 days post-ACT) of both NY-ESO-1/TCR-CD4 T cells and CD8 T cells upon ACT. Collectively, the in vitro and in vivo results show that NY-ESO-$1_{123–137}$/*DRB3*02:02*-TCR–engineered CD4 T cells are highly potent in controlling NY-ESO-1–expressing tumors.

DISCUSSION

In this study, we have identified a highly conserved NY-ESO-1 TCRαβ variable chain usage that confers potent antigen-specific effector functions against various tumor types. Moreover, gene transfer of

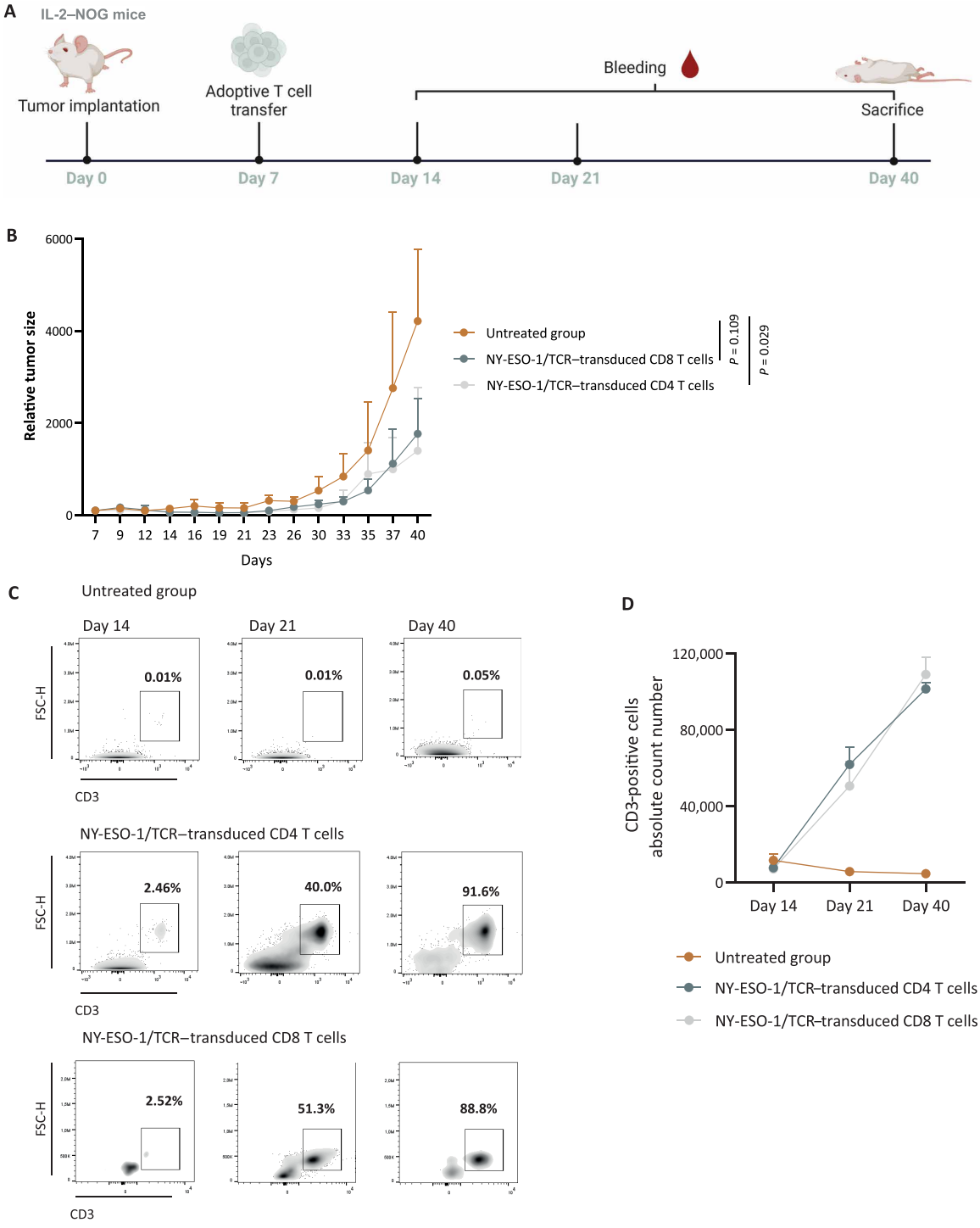

Fig. 8. Adoptive transfer of NY-ESO-1/TCR T cells in tumor-bearing IL-2–NOG mice. (**A**) Schematic of experimental strategy. (**B**) In vivo efficacy of adoptively transferred NY-ESO-1/TCR–transduced T cells against HLA-matched tumor xenografts (six mice per group). Statistical power was assessed using Kruskal-Wallis test. (**C**) Representative dot plots of human CD3 staining of the PBMCs of untreated mice and mice receiving NY-ESO-1/TCR–transduced CD4 T cells or NY-ESO-1/TCR–transduced CD8 T cells. (**D**) Monitoring of the frequency of persisting human T cells by flow cytometry (six mice per group).

such TCR in CD4 T cells confers robust cytotoxic capacity both in vitro and in vivo. Together, our data indicate strong potential for the clinical application of our TCR-engineered CD4 T cells targeting NY-ESO-1–expressing tumors in *HLA-DRB3*02:02*–positive patients, representing more than half of the Caucasian population. The discovery of a strong TCRαβ preferentially used in NY-ESO-$1_{123–137}$–specific CD4 T cells, particularly the recurrent TRAV8-4 and TRBV20-1 pair, raises intriguing questions about their origins and implications.

Previous vaccination studies in *HLA-DRB3*02:02*–positive patients with cancer using the NY-ESO-1 recombinant protein reported the induction of an immunodominant response characterized by the preferential expansion of proinflammatory type-1 NY-ESO-$1_{123–137}$–specific CD4 T cells (*18*). These findings also revealed marked differences between natural- and therapy-induced NY-ESO-1–specific CD8 T cell responses, where conserved but distinct TCRβ usage was reported (*24*) in the two settings. We extend these postimmunotherapy findings by reporting the expansion of NY-ESO-$1_{123–137}$–specific CD4 T cells in patients with advanced cancer exhibiting naturally occurring responses to NY-ESO-1, both in the peripheral blood and in tumor-infiltrated tissues. Biases in TCRα or TCRβ usage have been found in different diseases, spanning from autoimmunity to infection and cancer. These analyses were primarily performed in CD8 T cells (*25*), with only few examples in CD4 T cells relating to HLA-DRB1–restricted epitopes. In the well-known contexts of *HLA-A*02:01*–restricted Melan-A–specific (*26*) or yellow fever–specific (*27*) CD8 T cells, a strong TCR bias was already present in the naïve T cell population. However, in our case, it appears that a more limited TCRαβ skewing is observed in *HLA-DRB3*02:02*–positive HD's peripheral blood than in patients and not at all observed in CD4 T cells from the cord blood of *HLA-DRB3*02:02*–positive donors, strongly suggesting an antigen-driven expansion of the preferential TCR pair.

The presence of this TCR bias might be directly linked to the unusually strong cytotoxicity of these CD4 T cells. We hypothesized that pMHC/TCR affinity could partially explain this heightened cytotoxic potency, as reported for CD8 T cells, where the affinity and binding strength of a TCR to its cognate pMHC correlate with T cell effector functions (*28*). In line with this idea, our in silico analysis indicated that the *HLA-DRB3*02:02* molecule with the NY-ESO-1 peptide is predicted to foster more favorable contacts compared to Melan-A and hTERT peptides. Furthermore, we observed increased contacts of the TCR isolated from highly cytotoxic clones, both with the MHC-peptide complex and with the MHC molecule itself. This suggests that these T cells could engage in more favorable interactions between TCR, peptide, and MHC molecules, driving their preferential differentiation, polyfunctionality, and cytotoxic capacity, thereby explaining the TCR bias of the NY-ESO-$1_{123–137}$–specific CD4 T cell population. This heightened effector profile might be key to support the functional fitness of other immune cell types, e.g., CD8 T cells, and prevent their exhaustion, as recently reported (*4*).

In addition to the TCR variable chain usage bias, the high cytotoxic potency of our NY-ESO-1 clones might also be associated with a distinct differentiation state of the cells. When comparing clones with the same HLA restriction (i.e., *HLA-DRB3*02:02*) but different specificities (i.e., NY-ESO-1, hTERT, and Melan-A), we observed higher expression of PD-1, TIGIT, and VISTA alongside lower expression of CD57 in the cytotoxic NY-ESO-1–specific cells, as compared to the helper hTERT- and Melan-A–specific cells. While PD-1, TIGIT, and VISTA have been mainly associated with the suppression of effector T cell functions in cancer (*29*), the increased TIGIT expression in cytotoxic CD4 T cells might be related to a senescent phenotype with superior polyfunctionality, as reported for CD4 T cells in the transplantation setting (*30*). Similarly, reduced CD57 expression in natural killer cells (NK cells) was found to enhance cytotoxicity in patients, suggesting a compensatory mechanism to maintain immune function during disease (*31*).

Regarding cytotoxic molecules, we observed higher GZMB expression levels in NY-ESO-1–specific CD4 T clones, as compared to the Melan-A– and hTERT-specific ones, suggesting a greater killing potential. Of interest, although NY-ESO-1–reactive cells were generally highly cytotoxic, those originated from TILs/TILNs exhibited reduced target cell killing. The reduced presence of SLAMF7, previously identified as crucial in the cytotoxic process of CD4 T cells (*2*, *3*, *32*), along with increased expression of CTLA-4, 4-1BB, and OX40 in cells from TILs/TILNs, inversely correlated with cytotoxicity. This suggests that intracellular signaling from these receptors might directly affect target lysis. Further work should address how cytotoxicity might be optimally sustained in the tumor bed.

Together, TCR-engineered CD4 T cells targeting NY-ESO-$1_{123–137}$/*HLA-DRB3*02:02* offer a promising, novel, and presumably safe immunotherapeutic approach due to limited antigen expression on healthy tissues, which can be used to treat a relatively large proportion of patients with cancer. Our therapy could be used either alone or in combination with CD8 T cell based on immunotherapy or vaccination to further expand the immunodominant NY-ESO-$1_{123–137}$–specific CD4 T cell population. Future efforts should focus on editing these TCRs in other cell types. Alternatively, harnessing TCR-engineered NK cells may combine the innate properties of NK cells with the antigen specificity of the T cells, without the need of autologous cellular product preparation (*33*).

One potential limitation of our study is the use of in vitro expansion of T cell clones before TCR analysis. While direct ex vivo analysis is challenging, we acknowledge that the expansion process may influence the observed prevalence of specific clones, particularly high-affinity ones. This could introduce some bias in the assessment of clone prevalence. Despite this, we believe that the controls used in our study, which definitively demonstrate that the TRAV8-4 and TRBV20-1 biases are antigen associated, provide compelling evidence supporting the selective expansion of these clones. These controls effectively rule out alternative explanations and reinforce the antigen-driven nature of the observed biases.

MATERIALS AND METHODS

Lymphocyte isolation from cord blood, peripheral blood, tumor samples, and tumor-infiltrated lymph node samples

PBMCs from patients with stage III/IV melanoma and ovarian cancer and PBMCs from healthy donors (*34*) were obtained from the Department of Oncology, Centre Hospitalier Universitaire Vaudois (CHUV), Lausanne, Switzerland (NCT00112229, NCT00002669, and NCT00002763), and the Blood Transfusion Center, Lausanne, Switzerland, respectively. Blood was diluted with phosphate-buffered saline (PBS), and PBMCs were purified by density gradient centrifugation using Lymphoprep (STEMCELL). Mononuclear cells from cord blood and PBMCs from patients with lung cancer were obtained from O. Adotevi, University Hospital of Besançon (NCT02846103). TILs and TILNs were obtained after surgery from patients with melanoma from the Department of Oncology, University Hospital (CHUV), Lausanne, Switzerland (EC 2023-00186). Resected tumors were

enzymatically digested and were used as starting material for TIL/TILN generation, as previously reported (*35*).

Tumor cell lines

Melanoma cell lines (Me252, T333A, T672E, and NA8) were established from metastatic surgery specimens from patients with melanoma at the Department of Oncology, University Hospital (CHUV), Lausanne, Switzerland. The GEFI melanoma cell line was provided by M. P. Protti, San Raffaele Scientific Institute, Milan. Melanoma tumor cell lines were cultured in RPMI 1640 (Gibco) containing 10% fetal bovine serum (FBS; Gibco), 100 mM Hepes buffer (Gibco), penicillin (50 U/ml), and streptomycin (50 μg/ml; Thermo Fisher Scientific). Neuroblastoma cell lines (SH-EP and SKNSH) and a sarcoma cell line (U2OS) were obtained from the Department of Oncology, University Hospital (CHUV), Lausanne, Switzerland. Neuroblastoma tumor cell lines were cultured in Dulbecco's modified Eagle's medium (Gibco) containing 10% FBS, penicillin (50 U/ml), and streptomycin (50 μg/ml). The sarcoma tumor cell line was cultured in McCoy's 5a (Gibco) containing 15% FBS, penicillin (50 U/ml), and streptomycin (50 μg/ml).

Peptide synthesis

Peptides (table S1) were synthesized by the Peptide and Tetramer Core Facility, UNIL-CHUV, Epalinges, Switzerland, using INTAVIS synthesizers. All peptides were >90% pure as indicated by analytic mass spectrometry and high-performance liquid chromatography. The lyophilized peptides were diluted in pure dimethyl sulfoxide at 10 mM and stored at −20°C. This methodology was previously reported in (*2*).

HLA genotyping

Genomic DNA was extracted from cell samples using the DNeasy kit from QIAGEN. HLA typing was performed with the TruSight HLA v.2 Sequencing Panel from CareDx. Then, genomic DNA was used to amplify HLA genes by polymerase chain reaction (PCR). Nextera adapters were added by tagmentation, and the resulting libraries were sequenced on the MiniSeq instrument (Illumina). Sequencing data were analyzed with the Assign TruSight HLA v.2.1 Software. This methodology was previously reported in (*36*).

Identification of antigen-specific CD4 T cells and generation of T cell clones

PBMCs, TILs, and TILNs from *HLA-DRB3*02:02*–positive patients were thawed, and CD4 T cells were purified by positive selection using magnetic-activated cell sorter (MACS) isolation microbeads (Miltenyi Biotec). These cells were then stimulated with the indicated peptides (2 μM) and with the irradiated [30 Gy (gray)] autologous CD4-negative cell fraction in RPMI 1640 containing 8% of human serum (HS), 2 mM glutamine (Thermo Fisher Scientific), 1% (v/v) nonessential amino acids (Gibco), 50 μM 2β-mercaptoethanol (Gibco), penicillin (50 U/ml), and streptomycin (50 μg/ml) (8% HS RPMI 1640 medium). After 2 days of culture, 100 μl of 8% HS RPMI 1640 medium containing a final concentration of 100 U/ml of human recombinant IL-2 (Proleukine) was added. After 10 days of in vitro expansion, antigen-specific CD4 T cells were stained with fluorescent pMHCII multimers with an optimized protocol developed in-house (*37*). Cells were first resuspended in RPMI 1640 8% HS with 5 mM LacNac (Sigma-Aldrich) for 2 hours at 37°C and then resuspended in PBS containing 50 nM dasatinib (Sigma-Aldrich) for 30 min at 37°C. Multimer staining was performed using phycoerythrin (PE)–*HLA-DRB3*02:02* multimers, loaded with the indicated peptide (produced by the Peptide and Tetramer Core Facility, UNIL-CHUV, Epalinges, Switzerland), for 25 min at room temperature (RT). Surface staining was performed with anti-CD3 antibody (BV605, SP34-2, BD), anti-CD4 antibody (BV650, OKT4, BioLegend), and LIVE/DEAD Fixable Near-IR Dead Cell Stain (Thermo Fisher Scientific) for 20 min at RT. Last, a mouse anti-PE antibody (BioLegend) was added for 20 min at 4°C. Positive cells were sorted using a FACSAria II (BD Biosciences). Individual, sorted, and epitope-specific T cells were stimulated with phytohemagglutinin (1 μg/ml; Thermo Fisher Scientific) in the presence of irradiated (30 Gy) allogeneic PBMC feeder cells and IL-2 (100 U/ml) and plated in Terasaki plates for clone generation.

Generation of CIITA-transduced melanoma cell lines

Six hours before transfection, 293T cells (American Type Culture Collection) were seeded at 1.25×10^6 in 2 ml of 10% FBS RPMI 1640 medium per well in a six-well plate. 293T cells were transfected with 2.5 μg of total DNA (divided as 0.282 μg of pVSVG (vesicular stomatitis virus G glycoprotein), 0.846 μg of R874, and 1.125 μg of plasmid containing the human CIITA isoform 3 gene) using a mix of Lipofectamine 2000 (Invitrogen) and OptiMEM media (Invitrogen, Life Technologies, according to the manufacturer's instructions). The viral supernatant was harvested 48 hours post-transfection, and the supernatant was used directly on melanoma, lung, sarcoma, and neuroblastoma cell lines. MHCII positive cells were sorted using a FACSAria II (BD Biosciences) after staining with anti–HLA-DR/-DQ/-DP antibody [fluorescein isothiocyanate (FITC), Bu26, Abcam].

Lactate dehydrogenase cytotoxicity assay

The cytotoxic potential of the tumor-associated, antigen-specific (*38*), and *HLA-DRB3*02:02*–restricted CD4 T cell clones or TCR-transduced T cells was assessed against HLA-matched and HLA-mismatched tumor cell lines, as indicated. Target cells were incubated with effectors at different ratio (30:1, 15:1, 7.5:1, 3.8:1, and 1.7:1) for 24 hours at 37°C, in the presence or absence of the specific or irrelevant peptides (1 μM). Following the manufacturer's instructions, supernatants were collected and mixed with reaction mixture (CyQUANT LDH Cytotoxicity Assay Kit, Thermo Fisher Scientific) 30 min at RT in the dark. Stop solution was added, and the absorbances at 490 and 680 nm were measured to determine lactate dehydrogenase (LDH) activity. The percentage of specific lysis was calculated as follows: (experimental − effector spontaneous release − target spontaneous release) ÷ (target maximal release − target spontaneous release) × 100.

Cytokine secretion profiling by LEGENDplex analysis

Cytokine production by TAA-specific CD4 T cell clones was assessed after 24 hours of stimulation by the specific peptide at different concentrations (from 0 to 10 μM) to determine the half-maximal effective concentration. Supernatants were harvested, and the concentration of 12 cytokines (IL-5, IL-13, IL-2, IL-6, IL-9, IL-10, IFN-γ, TNF-α, IL-17A, IL-17F, IL-4, and IL-22) was measured using the LEGENDplex Human Th Panel (BioLegend). The beads were mixed with the supernatants, incubated for 2 hours at RT, washed, and incubated for 1 hour with detection antibodies. Streptavidin-PE was added and incubated for 30 min, and the beads were washed

and acquired using Attune NxT instrument (Thermo Fisher Scientific). Results were analyzed using the LEGENDplex Software Analysis Suite.

Multiparametric flow cytometry analysis of TAA-specific CD4 T cells and CD4 T cell clones

PBMCs, TILs, and TILNs or TAA-specific CD4 T cell clones were stained with a combination of antibodies: anti-CD3 (BV605, SP34-2, BD), anti-CD4 (BV650, OKT4, BioLegend), antiperforin (FITC, B-D48, BioLegend), anti–granzyme K (PerCP-efluor710, G3H69, eBioscience), anti–granzyme A (Alexa Fluor 700, CB9, BioLegend), anti-SLAMF7 (PE-Cy7, 162.1, BioLegend), anti–PD-1 (BV421, EH12.2H7, BioLegend), anti-CD57 (BV510, QA17A04, BioLegend), anti-VISTA (FITC, B7H5DS8, Invitrogen), anti-OX40 (PerCP-Cy5.5, Ber-ACT35, BioLegend), anti-41BB (Alexa Fluor 700, 4B4–1, BioLegend), anti-TIGIT (PE-Dazzle, A15153G, BioLegend), anti–CTLA-4 (PE-Cy5, BN13, BD), and LIVE/DEAD Fixable Near-IR Dead Cell Stain (Thermo Fisher Scientific). Data were acquired on Cytek Aurora and analyzed using FlowJo 10.8.1.

TCR sequencing

Following the procedures previously described in (*39*), mRNA was isolated from naïve cord blood CD4 T cells, memory CD4 T cells, TAA-specific CD4 T cells, and TAA-specific CD4 T cell clones using the Dynabeads mRNA DIRECT Purification Kit (Life Technologies) and was amplified using the MessageAmp II aRNA Amplification Kit (Ambion). First, strand cDNA was synthesized using SuperScript III (Thermo Fisher Scientific) and a collection of TRAV/TRBV-specific primers. TCRs were amplified by PCR (20 cycles with the Phusion from New England Biolabs), with a single primer pair binding to the constant region. MiniSeq instrument (Illumina) was lastly used for deep sequencing of the TCRα/TCRβ chains.

TCR/pMHC 3D structure modeling

The full sequence of the constant and variable domains of TCRα and TCRβ was reconstituted from V and J segment identifiers and from the CDR3 sequences using the IMGT/GENE-DB reference sequences (*40*) for TCR1, TCR2, and TCR3. Homology models of the three pMHC complexes (*HLA-DRB3*02:02* with the NY-ESO-1, hTERT, and Melan-A peptides) were generated using the Modeller program version 9 (*41*). On the basis of their sequence identity to HLA-DRA and *HLA-DRB3*02:02* and their resolution, the following experimental structures were retrieved from the Protein Data Bank (PDB) (*42*) and selected as templates for the homology modeling: 2q6w, 4h1l, 3c5j, and 1aqd. The sequence alignment between the MHC molecule and the templates was performed using MUSCLE (*43*). Because several positioning of the NY-ESO-1, hTERT, and Melan-A peptides in the MHC groove could be envisioned, the corresponding sequence alignments with the peptides present in the templates were generated and used as input to start the Modeller calculations. A total of 2000 models were generated for each pMHC complex and each possible peptide positioning. Models were scored according to the Discrete Optimized Potential Energy (DOPE) of Modeller (*41*) summed over all peptide residues and MHC residues in contact with them. For each peptide, the final pMHC model was selected as the one with the most favorable DOPE score. Homology models of the nine TCR-pMHC complexes (i.e., the three pMHC mentioned above in complex with TCR1, TCR2, or TCR3) were generated with the TCRmodel2 program (*44*) using default options, letting the approach automatically select the most appropriate templates. TCRmodel2 selected the following templates from the PDB:

1) TCR1: 4gkz, 6eh6, 6fra, and 3tf7 for TCRα and 3o4l, 1ymm, 2wbj, and 4dzb for TCRβ

2) TCR2: 4gkz, 6eh6, 6fra, and 3tf7 for TCRα and 1bd2, 4ftv, 6jxr, and 6rpb for TCRβ

3) TCR3: 4gkz, 6eh6, 6fra, and 3tf7 for TCRα and 6ovo, 6vmx, 6vxm, and 6ovn for TCRβ

Five models were generated for each of the nine TCR-pMHC complexes. In each case, it was verified that the positioning of the peptide in the MHC groove is identical between the models generated by Modeller and TCRmodel2. All models, for the three pMHC and nine TCR-pMHC complexes, were analyzed using the UCSF Chimera package (*45*) to determine the favorable molecular interactions between the peptide and the MHC and between the TCR and the pMHC residues. To account for protein flexibility, the five models generated by TCRmodel2 for each TCR-pMHC were used for this analysis. Residue numbering was generated by TCRmodel2. Molecular graphics was performed with the UCSF Chimera package.

TCR cloning and TCR transduction in primary human CD4 T cells

TCRα and TCRβ sequences were modified by replacing the human TCR constant regions with murine TCR constant regions and were cloned separately into pRRL vector under the control of an human phosphoglycerate kinase (hPGK) promoter, with the reporter gene green fluorescent protein. Then, TCRs were transduced into primary CD4 T cells previously isolated from HD PBMCs using MACS isolation microbeads (Miltenyi Biotec). On day 1, 293T cells were seeded at 1.25×10^6 in 2 ml of 10% FBS RPMI 1640 medium per well in a six-well plate. 293T cells were transfected with 2.5 μg of total DNA (divided as 0.282 μg of pVSVG, 0.846 μg of R874, and 1.125 μg of plasmid containing TCR sequences) using a mix of Lipofectamine 2000 (Invitrogen) and OptiMEM media (Invitrogen, Life Technologies, according to the manufacturer's instructions). The cells were incubated 48 hours at 37°C. On day 2, primary CD4 T cells were seeded at 1.5×10^6 in 2 ml of 8% HS RPMI 1640 medium + IL-2 (50 U/ml) in a 24-well plate. CD4 T cells were then activated 18 to 22 hours with anti-CD3 and anti-CD28 monoclonal antibody–coated beads (Invitrogen, Life Technologies) in a ratio of 1:2 of T cells to beads. On day 3, CD4 T cells were harvested, and beads were magnetically removed. T cells were then seeded at 1×10^6 in 2 ml of 8% HS RPMI 1640 medium + IL-2 (50 U/ml) in a six-well plate. The supernatant of the 293T cells containing the viral particles was harvested and was directly used on CD4 T cells. Cells were incubated for 3 days at 37°C. On day 4, transduced CD4 T cells were harvested and resuspended at 1×10^6 in 90 μl of OptiMEM (Invitrogen). Endogenous TCRs were knocked out by CRISPR-Cas9 technology. Two CRISPR mixes were prepared, one to knock out the TCRα chain [10 μg of Cas9 and 5 μg of *TRAC* (T Cell Receptor Alpha Constant) single guide RNA (sgRNA)] and one for the TCRβ chain (10 μg of Cas9 and 5 μg of *TRBC* (T Cell Receptor Beta Constant) sgRNA). Both were mixed and added to the cells, and electroporation was performed (Super Electroporator NEPA21 Type II). Transduced cells were sorted by multimer staining using a PE-*HLA-DRB3*02:02*/TAA multimer, as described above. Transduced CD4 T cells were cultured in 8% HS RPMI 1640 medium + IL-2 (50 U/ml) and IL-7 and IL-15 (10 ng/ml) (PeproTech).

ACT in immunodeficient IL-2–NOG mice

Following the procedures previously described in (*46*), IL-2–NOG mice from Taconic Biosciences were maintained in the animal facility at the University of Lausanne under specific pathogen–free status. Ten-week-old female mice were anesthetized with isoflurane and subcutaneously injected with 1×10^6 tumor cells (T333A). After 1 week, once the tumors became palpable, 5×10^6 human NY-ESO-$1_{123\text{-}137}$/TCR–transduced CD4 T cells were injected intravenously in the tail vein. To compare the efficacy of this treatment, one control group was injected with RPMI 1640 only (untreated group), and one group was injected with *HLA-A2*/NY-ESO-$1_{157\text{–}165}$/TCR–transduced CD8 T cells (*47*), provided by A. Harari. Tumor volumes were measured by caliper three times a week and calculated as follows: length × width. Blood was collected in the tail vein once a week. Blood was diluted with PBS, and PBMCs were purified by density gradient centrifugation using Lymphoprep (STEMCELL). Mice were euthanized by CO_2 inhalation before the tumor volume exceeded 1 cm^3 or when the state of the mice was affected over a certain threshold, defined by a scoresheet considering physical and behavioral parameters. After sacrifice, spleens, tumors, and blood were harvested and processed to isolate PBMCs. This study was approved by the Veterinary Authority of the Canton Vaud under the license 3746b and performed in accordance with Swiss ethical guidelines.

Statistical analysis

Statistical analyses were performed as indicated in the figure legends. For all analyses, *P* value less than 0.05 was considered as statistically significant and labeled with *, *P* value less than 0.01 was labeled with **, *P* value less than 0.001 was labeled with ***, and *P* value less than 0.0001 was labeled with ****. No significant differences were labeled with ns or left blank. Statistical analyses were performed using GraphPad Prism v.8.3.0.

Supplementary Materials

This PDF file includes:

Figs. S1 to S3
Tables S1 to S15

REFERENCES AND NOTES

1. D. J. Olson, K. Odunsi, Adoptive cell therapy for nonhematologic solid tumors. *J. Clin. Oncol.* **41**, 3397–3407 (2023).
2. A. Cachot, M. Bilous, Y. C. Liu, X. Li, M. Saillard, M. Cenerenti, G. A. Rockinger, T. Wyss, P. Guillaume, J. Schmidt, R. Genolet, G. Ercolano, M. P. Protti, W. Reith, K. Ioannidou, L. de Leval, J. A. Trapani, G. Coukos, A. Harari, D. E. Speiser, A. Mathis, D. Gfeller, H. Altug, P. Romero, C. Jandus, Tumor-specific cytolytic CD4 T cells mediate immunity against human cancer. *Sci. Adv.* **7**, eabe3348 (2021).
3. D. Y. Oh, S. S. Kwek, S. S. Raju, T. Li, E. McCarthy, E. Chow, D. Aran, A. Ilano, C. S. Pai, C. Rancan, K. Allaire, A. Burra, Y. Sun, M. H. Spitzer, S. Mangul, S. Porten, M. V. Meng, T. W. Friedlander, C. J. Ye, L. Fong, Intratumoral $CD4^+$ T cells mediate anti-tumor cytotoxicity in human bladder cancer. *Cell* **181**, 1612–1625.e13 (2020).
4. G. Espinosa-Carrasco, E. Chiu, A. Scrivo, P. Zumbo, A. Dave, D. Betel, S. W. Kang, H. J. Jang, M. D. Hellmann, B. M. Burt, H. S. Lee, A. Schietinger, Intratumoral immune triads are required for immunotherapy-mediated elimination of solid tumors. *Cancer Cell* **42**, 1202–1216.e8 (2024).
5. N. N. Hunder, H. Wallen, J. Cao, D. W. Hendricks, J. Z. Reilly, R. Rodmyre, A. Jungbluth, S. Gnjatic, J. A. Thompson, C. Yee, Treatment of metastatic melanoma with autologous $CD4^+$ T cells against NY-ESO-1. *N. Engl. J. Med.* **358**, 2698–2703 (2008).
6. E. Tran, S. Turcotte, A. Gros, P. F. Robbins, Y. C. Lu, M. E. Dudley, J. R. Wunderlich, R. P. Somerville, K. Hogan, C. S. Hinrichs, M. R. Parkhurst, J. C. Yang, S. A. Rosenberg, Cancer immunotherapy based on mutation-specific $CD4^+$ T cells in a patient with epithelial cancer. *Science* **344**, 641–645 (2014).
7. Y. C. Lu, L. L. Parker, T. Lu, Z. Zheng, M. A. Toomey, D. E. White, X. Yao, Y. F. Li, P. F. Robbins, S. A. Feldman, P. van der Bruggen, C. A. Klebanoff, S. L. Goff, R. M. Sherry, U. S. Kammula, J. C. Yang, S. A. Rosenberg, Treatment of patients with metastatic cancer using a major histocompatibility complex class II-restricted T-cell receptor targeting the cancer germline antigen MAGE-A3. *J. Clin. Oncol.* **35**, 3322–3329 (2017).
8. M. Ishihara, T. Ishida, N. Mizuki, H. Inoko, H. Ando, S. Ohno, Clinical features of sarcoidosis in relation to HLA distribution and HLA-DRB3 genotyping by PCR-RFLP. *Br. J. Ophthalmol.* **79**, 322–325 (1995).
9. R. A. Morgan, M. E. Dudley, J. R. Wunderlich, M. S. Hughes, J. C. Yang, R. M. Sherry, R. E. Royal, S. L. Topalian, U. S. Kammula, N. P. Restifo, Z. Zheng, A. Nahvi, C. R. de Vries, L. J. Rogers-Freezer, S. A. Mavroukakis, S. A. Rosenberg, Cancer regression in patients after transfer of genetically engineered lymphocytes. *Science* **314**, 126–129 (2006).
10. M. R. Parkhurst, J. C. Yang, R. C. Langan, M. E. Dudley, D. A. Nathan, S. A. Feldman, J. L. Davis, R. A. Morgan, M. J. Merino, R. M. Sherry, M. S. Hughes, U. S. Kammula, G. Q. Phan, R. M. Lim, S. A. Wank, N. P. Restifo, P. F. Robbins, C. M. Laurencot, S. A. Rosenberg, T cells targeting carcinoembryonic antigen can mediate regression of metastatic colorectal cancer but induce severe transient colitis. *Mol. Ther.* **19**, 620–626 (2011).
11. G. P. Linette, E. A. Stadtmauer, M. V. Maus, A. P. Rapoport, B. L. Levine, L. Emery, L. Litzky, A. Bagg, B. M. Carreno, P. J. Cimino, G. K. Binder-Scholl, D. P. Smethurst, A. B. Gerry, N. J. Pumphrey, A. D. Bennett, J. E. Brewer, J. Dukes, J. Harper, H. K. Tayton-Martin, B. K. Jakobsen, N. J. Hassan, M. Kalos, C. H. June, Cardiovascular toxicity and titin cross-reactivity of affinity-enhanced T cells in myeloma and melanoma. *Blood* **122**, 863–871 (2013).
12. Y. T. Chen, M. J. Scanlan, U. Sahin, O. Tureci, A. O. Gure, S. Tsang, B. Williamson, E. Stockert, M. Pfreundschuh, L. J. Old, A testicular antigen aberrantly expressed in human cancers detected by autologous antibody screening. *Proc. Natl. Acad. Sci. U.S.A.* **94**, 1914–1918 (1997).
13. A. A. Jungbluth, Y. T. Chen, E. Stockert, K. J. Busam, D. Kolb, K. Iversen, K. Coplan, B. Williamson, N. Altorki, L. J. Old, Immunohistochemical analysis of NY-ESO-1 antigen expression in normal and malignant human tissues. *Int. J. Cancer* **92**, 856–860 (2001).
14. P. Baumgaertner, C. Costa Nunes, A. Cachot, H. Maby-El Hajjami, L. Cagnon, M. Braun, L. Derre, J. P. Rivals, D. Rimoldi, S. Gnjatic, S. Abed Maillard, P. Marcos Mondejar, M. P. Protti, E. Romano, O. Michielin, P. Romero, D. E. Speiser, C. Jandus, Vaccination of stage III/IV melanoma patients with long NY-ESO-1 peptide and CpG-B elicits robust $CD8^+$ and $CD4^+$ T-cell responses with multiple specificities including a novel DR7-restricted epitope. *Onco Targets Ther* **5**, e1216290 (2016).
15. P. F. Robbins, S. H. Kassim, T. L. Tran, J. S. Crystal, R. A. Morgan, S. A. Feldman, J. C. Yang, M. E. Dudley, J. R. Wunderlich, R. M. Sherry, U. S. Kammula, M. S. Hughes, N. P. Restifo, M. Raffeld, C. C. Lee, Y. F. Li, M. El-Gamil, S. A. Rosenberg, A pilot trial using lymphocytes genetically engineered with an NY-ESO-1-reactive T-cell receptor: Long-term follow-up and correlates with response. *Clin. Cancer Res.* **21**, 1019–1027 (2015).
16. A. P. Rapoport, E. A. Stadtmauer, G. K. Binder-Scholl, O. Goloubeva, D. T. Vogl, S. F. Lacey, A. Z. Badros, A. Garfall, B. Weiss, J. Finklestein, I. Kulikovskaya, S. K. Sinha, S. Kronsberg, M. Gupta, S. Bond, L. Melchiori, J. E. Brewer, A. D. Bennett, A. B. Gerry, N. J. Pumphrey, D. Williams, H. K. Tayton-Martin, L. Ribeiro, T. Holdich, S. Yanovich, N. Hardy, J. Yared, N. Kerr, S. Philip, S. Westphal, D. L. Siegel, B. L. Levine, B. K. Jakobsen, M. Kalos, C. H. June, NY-ESO-1-specific TCR-engineered T cells mediate sustained antigen-specific antitumor effects in myeloma. *Nat. Med.* **21**, 914–921 (2015).
17. P. F. Robbins, R. A. Morgan, S. A. Feldman, J. C. Yang, R. M. Sherry, M. E. Dudley, J. R. Wunderlich, A. V. Nahvi, L. J. Helman, C. L. Mackall, U. S. Kammula, M. S. Hughes, N. P. Restifo, M. Raffeld, C. C. Lee, C. L. Levy, Y. F. Li, M. El-Gamil, S. L. Schwarz, C. Laurencot, S. A. Rosenberg, Tumor regression in patients with metastatic synovial cell sarcoma and melanoma using genetically engineered lymphocytes reactive with NY-ESO-1. *J. Clin. Oncol.* **29**, 917–924 (2011).
18. G. Bioley, C. Dousset, A. Yeh, B. Dupont, N. Bhardwaj, G. Mears, L. J. Old, M. Ayyoub, D. Valmori, Vaccination with recombinant NY-ESO-1 protein elicits immunodominant HLA-DR52b-restricted $CD4^+$ T cell responses with a conserved T cell receptor repertoire. *Clin. Cancer Res.* **15**, 4467–4474 (2009).
19. J. Racle, J. Michaux, G. A. Rockinger, M. Arnaud, S. Bobisse, C. Chong, P. Guillaume, G. Coukos, A. Harari, C. Jandus, M. Bassani-Sternberg, D. Gfeller, Robust prediction of HLA class II epitopes by deep motif deconvolution of immunopeptidomes. *Nat. Biotechnol.* **37**, 1283–1286 (2019).
20. R. S. Accolla, E. Ramia, A. Tedeschi, G. Forlani, CIITA-driven MHC class II expressing tumor cells as antigen presenting cell performers: Toward the construction of an optimal anti-tumor vaccine. *Front. Immunol.* **10**, 1806 (2019).
21. J. L. Tanyi, S. Bobisse, E. Ophir, S. Tuyaerts, A. Roberti, R. Genolet, P. Baumgartner, B. J. Stevenson, C. Iseli, D. Dangaj, B. Czerniecki, A. Semilietof, J. Racle, A. Michel, I. Xenarios, C. Chiang, D. S. Monos, D. A. Torigian, H. L. Nisenbaum, O. Michielin, C. H. June, B. L. Levine, D. J. Powell Jr., D. Gfeller, R. Mick, U. Dafni, V. Zoete, A. Harari, G. Coukos, L. E. Kandalaft, Personalized cancer vaccine effectively mobilizes antitumor T cell immunity in ovarian cancer. *Sci. Transl. Med.* **10**, eaao5931 (2018).
22. S. Bobisse, R. Genolet, A. Roberti, J. L. Tanyi, J. Racle, B. J. Stevenson, C. Iseli, A. Michel, M. A. Le Bitoux, P. Guillaume, J. Schmidt, V. Bianchi, D. Dangaj, C. Fenwick, L. Derre, I. Xenarios, O. Michielin, P. Romero, D. S. Monos, V. Zoete, D. Gfeller, L. E. Kandalaft,

G. Coukos, A. Harari, Sensitive and frequent identification of high avidity neo-epitope specific CD8$^+$ T cells in immunotherapy-naive ovarian cancer. *Nat. Commun.* **9**, 1092 (2018).
23. I. Katano, T. Takahashi, R. Ito, T. Kamisako, T. Mizusawa, Y. Ka, T. Ogura, H. Suemizu, Y. Kawakami, M. Ito, Predominant development of mature and functional human NK cells in a novel human IL-2-producing transgenic NOG mouse. *J. Immunol.* **194**, 3513–3525 (2015).
24. F. A. Le Gal, M. Ayyoub, V. Dutoit, V. Widmer, E. Jager, J. C. Cerottini, P. Y. Dietrich, D. Valmori, Distinct structural TCR repertoires in naturally occurring versus vaccine-induced CD8$^+$ T-cell responses to the tumor-specific antigen NY-ESO-1. *J. Immunother.* **28**, 252–257 (2005).
25. J. J. Miles, D. C. Douek, D. A. Price, Bias in the αβ T-cell repertoire: Implications for disease pathogenesis and vaccination. *Immunol. Cell Biol.* **89**, 375–387 (2011).
26. M. J. Pittet, D. Valmori, P. R. Dunbar, D. E. Speiser, D. Lienard, F. Lejeune, K. Fleischhauer, V. Cerundolo, J. C. Cerottini, P. Romero, High frequencies of naive Melan-A/MART-1-specific CD8$^+$ T cells in a large proportion of human histocompatibility leukocyte antigen (HLA)-A2 individuals. *J. Exp. Med.* **190**, 705–716 (1999).
27. A. Bovay, V. Zoete, G. Dolton, A. M. Bulek, D. K. Cole, P. J. Rizkallah, A. Fuller, K. Beck, O. Michielin, D. E. Speiser, A. K. Sewell, S. A. Fuertes Marraco, T cell receptor α variable 12-2 bias in the immunodominant response to yellow fever virus. *Eur. J. Immunol.* **48**, 258–272 (2018).
28. M. Allard, B. Couturaud, L. Carretero-Iglesia, M. N. Duong, J. Schmidt, G. C. Monnot, P. Romero, D. E. Speiser, M. Hebeisen, N. Rufer, TCR-ligand dissociation rate is a robust and stable biomarker of CD8$^+$ T cell potency. *JCI Insight* **2**, e92570 (2017).
29. J. M. Chauvin, H. M. Zarour, TIGIT in cancer immunotherapy. *J. Immunother. Cancer* **8**, e000957 (2020).
30. A. C. J. van der List, N. H. R. Litjens, M. Klepper, M. G. H. Betjes, Expression of senescence marker TIGIT identifies polyfunctional donor-reactive CD4$^+$ T cells preferentially lost after kidney transplantation. *Front. Immunol.* **12**, 656846 (2021).
31. B. Liu, G. X. Yang, Y. Sun, T. Tomiyama, W. Zhang, P. S. C. Leung, X. S. He, S. Dhaliwal, P. Invernizzi, M. E. Gershwin, C. L. Bowlus, Decreased CD57 expression of natural killer cells enhanced cytotoxicity in patients with primary sclerosing cholangitis. *Front. Immunol.* **13**, 912961 (2022).
32. A. Chryplewicz, J. Scotton, M. Tichet, A. Zomer, K. Shchors, J. A. Joyce, K. Homicsko, D. Hanahan, Cancer cell autophagy, reprogrammed macrophages, and remodeled vasculature in glioblastoma triggers tumor immunity. *Cancer Cell* **40**, 1111–1127.e9 (2022).
33. T. J. Laskowski, A. Biederstadt, K. Rezvani, Natural killer cells in antitumour adoptive cell immunotherapy. *Nat. Rev. Cancer* **22**, 557–575 (2022).
34. Z. Asadzadeh, H. Mohammadi, E. Safarzadeh, M. Hemmatzadeh, A. Mahdian-Shakib, F. Jadidi-Niaragh, G. Azizi, B. Baradaran, The paradox of Th17 cell functions in tumor immunity. *Cell. Immunol.* **322**, 15–25 (2017).
35. P. O. Gannon, A. Harari, A. Auger, C. Murgues, V. Zangiacomi, O. Rubin, K. Ellefsen Lavoie, L. Guillemot, B. Navarro Rodrigo, T. Nguyen-Ngoc, S. Rusakiewicz, L. Rossier, C. Boudousquie, P. Baumgaertner, S. Zimmermann, L. Trueb, E. M. Iancu, C. Sempoux, N. Demartines, G. Coukos, L. E. Kandalaft, Development of an optimized closed and semi-automatic protocol for good manufacturing practice manufacturing of tumor-infiltrating lymphocytes in a hospital environment. *Cytotherapy* **22**, 780–791 (2020).
36. C. Chong, M. Muller, H. Pak, D. Harnett, F. Huber, D. Grun, M. Leleu, A. Auger, M. Arnaud, B. J. Stevenson, J. Michaux, I. Bilic, A. Hirsekorn, L. Calviello, L. Simo-Riudalbas, E. Planet, J. Lubinski, M. Bryskiewicz, M. Wiznerowicz, I. Xenarios, L. Zhang, D. Trono, A. Harari, U. Ohler, G. Coukos, M. Bassani-Sternberg, Integrated proteogenomic deep sequencing and analytics accurately identify non-canonical peptides in tumor immunopeptidomes. *Nat. Commun.* **11**, 1293 (2020).
37. G. A. Rockinger, P. Guillaume, A. Cachot, M. Saillard, D. E. Speiser, G. Coukos, A. Harari, P. J. Romero, J. Schmidt, C. Jandus, Optimized combinatorial pMHC class II multimer labeling for precision immune monitoring of tumor-specific CD4 T cells in patients. *J. Immunother. Cancer* **8**, e000435 (2020).
38. E. Wargowski, L. E. Johnson, J. C. Eickhoff, L. Delmastro, M. J. Staab, G. Liu, D. G. McNeel, Prime-boost vaccination targeting prostatic acid phosphatase (PAP) in patients with metastatic castration-resistant prostate cancer (mCRPC) using sipuleucel-T and a DNA vaccine. *J. Immunother. Cancer* **6**, 21 (2018).
39. R. Genolet, S. Bobisse, J. Chiffelle, M. Arnaud, R. Petremand, L. Queiroz, A. Michel, P. Reichenbach, J. Cesbron, A. Auger, P. Baumgaertner, P. Guillaume, J. Schmidt, M. Irving, L. E. Kandalaft, D. E. Speiser, G. Coukos, A. Harari, TCR sequencing and cloning methods for repertoire analysis and isolation of tumor-reactive TCRs. *Cell Rep. Methods* **3**, 100459 (2023).
40. V. Giudicelli, D. Chaume, M. P. Lefranc, IMGT/GENE-DB: A comprehensive database for human and mouse immunoglobulin and T cell receptor genes. *Nucleic Acids Res.* **33**, D256–D261 (2005).
41. B. Webb, A. Sali, Comparative protein structure modeling using MODELLER. *Curr. Protoc. Bioinformatics* **54**, 5.6.1–5.6.37 (2016).
42. P. W. Rose, A. Prlic, A. Altunkaya, C. Bi, A. R. Bradley, C. H. Christie, L. D. Costanzo, J. M. Duarte, S. Dutta, Z. Feng, R. K. Green, D. S. Goodsell, B. Hudson, T. Kalro, R. Lowe, E. Peisach, C. Randle, A. S. Rose, C. Shao, Y. P. Tao, Y. Valasatava, M. Voigt, J. D. Westbrook, J. Woo, H. Yang, J. Y. Young, C. Zardecki, H. M. Berman, S. K. Burley, The RCSB Protein Data Bank: Integrative view of protein, gene and 3D structural information. *Nucleic Acids Res.* **45**, D271–D281 (2017).
43. R. C. Edgar, MUSCLE: Multiple sequence alignment with high accuracy and high throughput. *Nucleic Acids Res.* **32**, 1792–1797 (2004).
44. R. Yin, H. V. Ribeiro-Filho, V. Lin, R. Gowthaman, M. Cheung, B. G. Pierce, TCRmodel2: High-resolution modeling of T cell receptor recognition using deep learning. *Nucleic Acids Res.* **51**, W569–W576 (2023).
45. E. F. Pettersen, T. D. Goddard, C. C. Huang, G. S. Couch, D. M. Greenblatt, E. C. Meng, T. E. Ferrin, UCSF Chimera—A visualization system for exploratory research and analysis. *J. Comput. Chem.* **25**, 1605–1612 (2004).
46. M. Arnaud, J. Chiffelle, R. Genolet, B. Navarro Rodrigo, M. A. S. Perez, F. Huber, M. Magnin, T. Nguyen-Ngoc, P. Guillaume, P. Baumgaertner, C. Chong, B. J. Stevenson, D. Gfeller, M. Irving, D. E. Speiser, J. Schmidt, V. Zoete, L. E. Kandalaft, M. Bassani-Sternberg, S. Bobisse, G. Coukos, A. Harari, Sensitive identification of neoantigens and cognate TCRs in human solid tumors. *Nat. Biotechnol.* **40**, 656–660 (2022).
47. M. Hebeisen, J. Schmidt, P. Guillaume, P. Baumgaertner, D. E. Speiser, I. Luescher, N. Rufer, Identification of rare high-avidity, tumor-reactive CD8$^+$ T cells by monomeric TCR-ligand off-rates measurements on living cells. *Cancer Res.* **75**, 1983–1991 (2015).

Acknowledgments: We thank the patients and healthy donors for participating in this study. We thank the flow cytometry and animal facilities of the Universities of Lausanne and Geneva for excellent technical assistance. We thank M. P. Protti (San Raffaele Scientific Institute, Milan) for sharing the GEFI tumor cell line. **Funding:** This work was supported by Fondazione San Salvatore (C.J., A.H., and D.G.), ISREC-Tandem Grant (C.J., F.C., and G.C.), Swisslife Jubiläumstiftung (M.S.), UNIGE-iGE3 PhD fellowship (M.C.), and SNFS PR00P3-179727 (C.J.).
Author contributions: Writing—original draft: M.S., C.J., G.C., Pe.R., and O.A. Conceptualization: M.S., C.J., F.C., G.C., and Pe.R. Investigation: M.S., C.J., Pa.R., V.Z., J.R, D.E.S., M.H., Pe.R., L.Q., J.C., and M.C. Writing—review and editing: M.S., C.J., F.C., V.Z., D.E.S., R.R., J.V., G.C., J.R., Pe.R., Z.S., O.M., and M.I. Methodology: M.S., C.J., Pa.R., V.Z., J.R., Pe.R., J.C., and M.I. Resources: C.J., F.C., Pa.R., V.Z., D.E.S., J.S., R.R., D.G., J.V., A.H., G.C., R.G., J.-P.R., O.M., J.C., M.I., P.G., and O.A. Funding acquisition: M.S., C.J., F.C., G.C., and M.C. Data curation: M.S., C.J., and Z.S. Validation: M.S., C.J., F.C., Pa.R., and M.C. Supervision: M.S., C.J., D.G., Pe.R., and M.I. Formal analysis: M.S., C.J., V.Z., and Z.S. Software: Z.S. Project administration: M.S., C.J., and Pe.R. Visualization: M.S., C.J., F.C., V.Z., J.R., Pe.R., Z.S., J.C., and M.C. **Competing interests:** UNIL and Ludwig Institute for Cancer Research have filed for patent protection on TCR sequencing technology used herein. R.G. is named as inventor on this patent. C.J., M.S., P.G., R.G., and Pe.R. are named as inventors on a provisional patent application based on certain subject matter contained in this article. The patent was filed on 28 March 2025 by the Ludwig Institute for Cancer Research (serial no. US63/779,551). Pe.R. is currently used by Novigenix SA, Lausanne, Switzerland. Pe.R. serves on the Scientific Advisory Boards of Transgene (Strasbourg, France), MPC Therapeutics (Geneva, Switzerland), and EsoBiotec (Brussels, Belgium). These affiliations are disclosed in the interest of full transparency and do not influence the content of this manuscript. All other authors declare that they have no competing interests. **Data and materials availability:** All data needed to evaluate the conclusions in the paper are present in the paper and/or the Supplementary Materials.

Submitted 12 November 2024
Accepted 22 May 2025
Published 27 June 2025
10.1126/sciadv.adu5754